Chapter 13

Angular Dependence of Scattering

Within the framework of this book all the information about elastic scattering by small particles is contained in the 4×4 scattering matrix (3.16); each of its 16 elements is an angle-dependent function of wavelength, particle size, shape, and composition. There is so much information in the complete scattering matrix, however, that only recently have the properties of all its elements begun to be investigated. Most theoretical and experimental work has been limited to scattering of unpolarized or linearly polarized light. Because of this, the present chapter is arranged as follows: in Sections 13.1 through 13.5 the incident light is unpolarized or linearly polarized; this restriction is removed in Sections 13.6 through 13.8. In Section 13.1 we discuss calculated scattering by spheres to give the reader some feeling for the various effects that can occur. Measurement techniques are then treated briefly in Sections 13.2 and 13.3. This is followed in Section 13.4 by calculations interspersed with measurements on spherical and nonspherical systems. Section 13.5 treats an important application: the sizing of particles by light scattering. Section 13.6 is somewhat of a digression: symmetry properties of the scattering matrix. Measurement techniques for the complete scattering matrix are given in Section 13.7, and results of measurements in Section 13.8. Section 13.9, the concluding section, summarizes the differences and similarities between spherical and nonspherical particles, partly in an attempt to answer the important practical question: To what extent is Mie theory applicable to nonspherical particles?

13.1 SCATTERING OF UNPOLARIZED AND LINEARLY POLARIZED LIGHT

The maximum amount of information about scattering by any particle or collection of particles is contained in all the elements of the 4×4 scattering matrix (3.16), which will be treated in more generality later in this chapter. Most measurements and calculations, however, are restricted to unpolarized or linearly polarized light incident on a collection of randomly oriented particles with an internal plane of symmetry (no optical activity, for example). In such instances, the relevant matrix elements are those in the upper left-hand 2×2 block of the scattering matrix, which has the symmetry shown below (see, e.g.,

Perrin, 1942, and Section 13.6):

$$\begin{pmatrix} I_s \\ Q_s \\ U_s \\ V_s \end{pmatrix} = \frac{1}{k^2 r^2} \left(\begin{array}{cc:c} S_{11} & S_{12} & \\ S_{12} & S_{22} & 0 \\ \hdashline & 0 & \end{array}\right) \begin{pmatrix} I_i \\ Q_i \\ U_i \\ V_i \end{pmatrix}. \tag{13.1}$$

Although we have chosen to emphasize the more common Stokes parameters (I, Q, U, V), the system $(I_\parallel, I_\perp, Q, V)$ is more suited to measurements in which linear polarizers are interposed in the incident and scattered beams. In the latter system, the Stokes parameters are defined by

$$I_\parallel = \langle E_\parallel E_\parallel^* \rangle, \qquad I_\perp = \langle E_\perp E_\perp^* \rangle,$$

in place of (2.84); U and V are the same in both systems. In the $(I_\parallel, I_\perp, U, V)$ system the scattering matrix corresponding to (13.1) is

$$\begin{pmatrix} I_{\parallel s} \\ I_{\perp s} \\ U_s \\ V_s \end{pmatrix} = \frac{1}{k^2 r^2} \left(\begin{array}{cc:c} Q_{11} & Q_{12} & \\ Q_{12} & Q_{22} & 0 \\ \hdashline & 0 & \end{array}\right) \begin{pmatrix} I_{\parallel i} \\ I_{\perp i} \\ U_i \\ V_i \end{pmatrix}.$$

The matrix elements in the two systems are related by

$$S_{11} = \tfrac{1}{2}(Q_{11} + 2Q_{12} + Q_{22}), \qquad Q_{11} = \tfrac{1}{2}(S_{11} + 2S_{12} + S_{22}),$$

$$S_{12} = \tfrac{1}{2}(Q_{11} - Q_{22}), \qquad Q_{12} = \tfrac{1}{2}(S_{11} - S_{22}),$$

$$S_{22} = \tfrac{1}{2}(Q_{11} - 2Q_{12} + Q_{22}), \qquad Q_{22} = \tfrac{1}{2}(S_{11} - 2S_{12} + S_{22}).$$

13.1.1 A Few Definitions

The scattered irradiances per unit incident irradiance (dimensionless irradiances) for incident light parallel and perpendicular to the scattering plane are (omitting $k^2 r^2$)

$$i_\parallel = S_{11} + S_{12} = Q_{11} + Q_{12},$$

$$i_\perp = S_{11} - S_{12} = Q_{22} + Q_{12},$$

and the dimensionless scattered irradiance for incident unpolarized light is

$$i = \frac{i_\parallel + i_\perp}{2} = S_{11}.$$

Other quantities commonly measured are the *degree of linear polarization* P of the scattered light for incident unpolarized light

$$P = -\frac{S_{12}}{S_{11}} = \frac{Q_{22} - Q_{11}}{Q_{11} + 2Q_{12} + Q_{22}},$$

and the *cross polarization*

$$Q_{12} = \tfrac{1}{2}(S_{11} - S_{22}),$$

which is measured by inserting linear polarizers fore and aft of the scattering medium, one with its axis parallel and the other with its axis perpendicular to the scattering plane; the order of the polarizers is unimportant for the special scattering matrix (13.1).

With the programs in the appendixes one can compute elements of the scattering matrix for spheres and, consequently, all the quantities defined in the preceding paragraph. The cross polarization vanishes for spherical particles, and the following relations hold:

$$P = \frac{Q_{22} - Q_{11}}{Q_{22} + Q_{11}}, \qquad i_{\parallel} = Q_{11}, \quad i_{\perp} = Q_{22}.$$

There are many other angle-dependent scattering functions in the scientific literature, which is a source of endless confusion. In the hope that it will help the confused—among whom we count ourselves—to reconcile the notation and terminology of various authors, some of the more commonly encountered functions are expressed in our notation.

The *differential scattering cross section* $dC_{\text{sca}}/d\Omega$, a familiar quantity in atomic physics, is defined as the energy scattered per unit time into a unit solid angle about a direction $\hat{\Omega}$—which may be specified by two angles, the scattering angle θ and the azimuthal angle ϕ (see Fig. 3.3)—for unit incident irradiance. It is expressed in terms of the scattered irradiance $I_s(\theta, \phi)$, the incident irradiance I_i, and the distance r to the detector as

$$\frac{dC_{\text{sca}}}{d\Omega} = \frac{r^2 I_s}{I_i}. \tag{13.2}$$

($dC_{\text{sca}}/d\Omega$ should not be interpreted as the derivative of a function of Ω; it is *formally* written as a derivative merely as an aid to memory). Although the quantity on the right side of (13.2) is often referred to as the "Rayleigh ratio," we shall avoid this term in favor of the more descriptive term (for physicists at least) differential scattering cross section. If the incident light is unpolarized

$$\frac{dC_{\text{sca}}}{d\Omega} = \frac{S_{11}}{k^2} = \frac{i_{\parallel} + i_{\perp}}{2k^2}.$$

For an isotropic medium such as a collection of many randomly oriented particles, which may themselves be anisotropic, the scattered irradiance and hence the differential scattering cross section is independent of ϕ.

The differential scattering cross section divided by the total scattering cross section

$$p = \frac{1}{C_{sca}} \frac{dC_{sca}}{d\Omega} \tag{13.3}$$

is called the *phase function*, a term originating in the phases of astronomical bodies. The phase function (13.3) agrees with that of van de Hulst (1957), but differs by a factor 4π from phase functions of other authors (e.g., Rozenberg, 1960; Hansen and Travis, 1974).

13.1.2 Scattering by Spheres

One example of calculated angular scattering by a sphere has been given already (Fig. 4.9). To further develop understanding of scattering by spheres, we display in various ways $i_{\parallel}$, $i_{\perp}$, and P for a sequence of spheres of increasing size in Figs. 13.1–13.3. Readers are encouraged to use the program in Appendix A to devise their own examples.

Calculations for spheres with optical constants appropriate to water at visible wavelengths are shown in Fig. 13.1; $i_{\parallel}$ and $i_{\perp}$ are plotted on the left, P on the right. Similar results for spheres with refractive index $m = 1.55 + i0.0$, which corresponds approximately to fused quartz in the visible region, are shown in Fig. 13.2.

For small size parameters, the familiar Rayleigh (see Section 5.1) scattering patterns are obtained: perpendicularly polarized light is scattered isotropically, while light polarized parallel to the scattering plane vanishes at a scattering angle of 90°; as a consequence, incident unpolarized light is completely polarized at 90°. For all sizes, $i_{\parallel} = i_{\perp}$ at 0° and 180°: the two polarizations are indistinguishable in these directions because of symmetry; in other directions, the scattering plane enforces a distinction. Polar plots of scattering functions are shown in Fig. 13.3 for various water droplets; no new information is contained in these plots, but they can evoke sharper physical images.

The first deviations from Rayleigh theory appear as forward–backward asymmetry, with more light being scattered in forward directions; also, peak polarization decreases and shifts to larger angles. As the size is increased further, the asymmetry becomes more pronounced and the dominant forward-scattering lobe narrows. A concomitant of an increase in size is more undulations, as if new peaks appear in the backscattering direction and move forward. For large particles, the increased complexity of scattering is an indicator of its extreme sensitivity to size. Thus, comparison of measured scattering with sets of calculations is a possible means of accurately sizing spheres. For a given refractive index, the number of peaks in the scattering pattern gives a fairly good measure of the sphere radius. This sensitivity to radius, however, causes structure to be obliterated as the size dispersion in a collection of particles increases, giving rise to much smoother patterns.

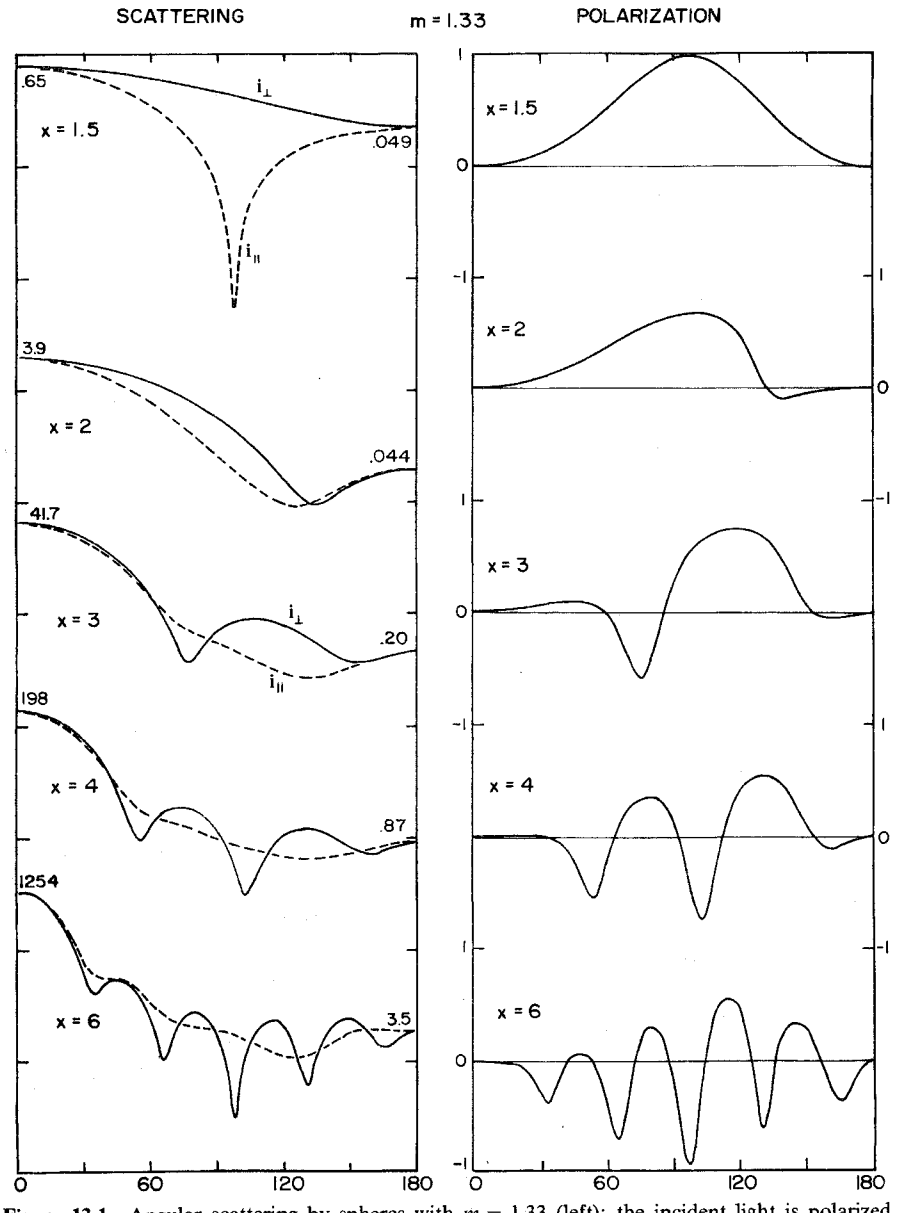

Figure 13.1 Angular scattering by spheres with $m = 1.33$ (left); the incident light is polarized parallel (---) or perpendicular (——) to the scattering plane. On the right is the degree of polarization of scattered light for incident unpolarized light.

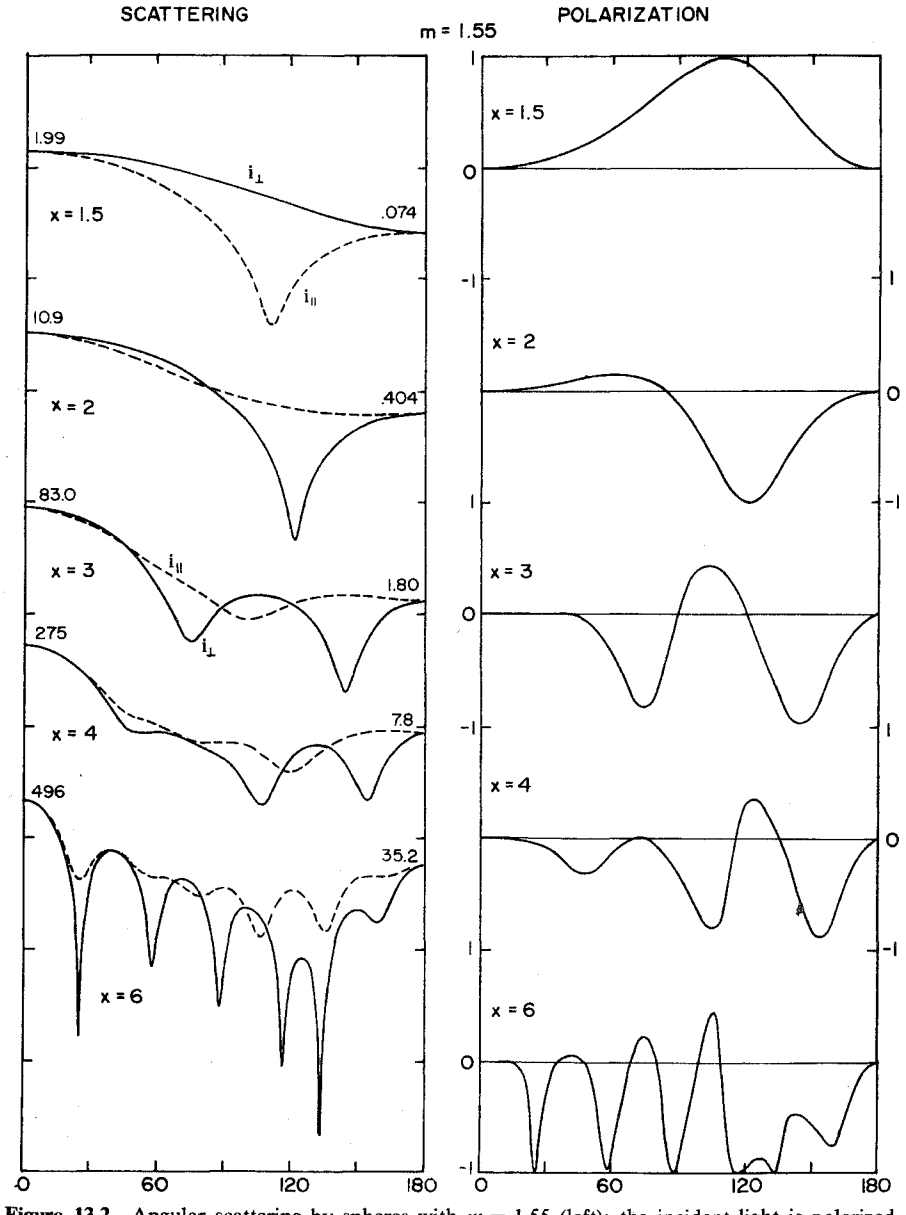

Figure 13.2 Angular scattering by spheres with $m = 1.55$ (left); the incident light is polarized parallel (---) or perpendicular (——) to the scattering plane. On the right is the degree of polarization of scattered light for incident unpolarized light.

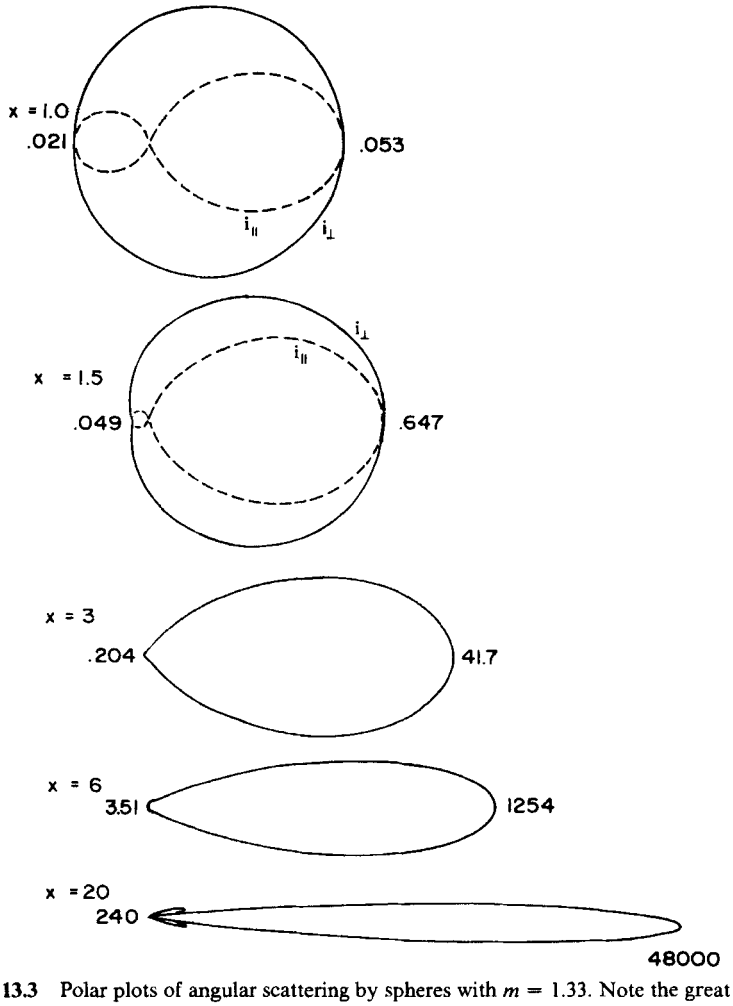

Figure 13.3 Polar plots of angular scattering by spheres with $m = 1.33$. Note the great change in scale: as x increases by 20 forward-to-backward scattering increases by about 1000.

Calculations of Hansen and Travis (1974) for a distribution of sizes are shown in Fig. 13.4; the size parameters are distributed according to $n(x) = x^6\exp(-9x/x_{\text{eff}})$. At visible wavelengths the three effective size parameters x_{eff} correspond to radii of about 20 μm, 80 μm, and 0.3 mm; this covers a range of sizes found in fogs and clouds. All curves show the relatively smooth behavior characteristic of a distribution of sizes, in contrast with the highly structured curves for single spheres. Scattering is strongly peaked in the forward direction; the forward (diffraction) lobe becomes increasingly confined to smaller angles as x_{eff} increases from 37.5 to 600. For $m = 1.33$ (water), two peaks develop in the region between 130 and 140°; these are the primary ($\theta \simeq 137°$)

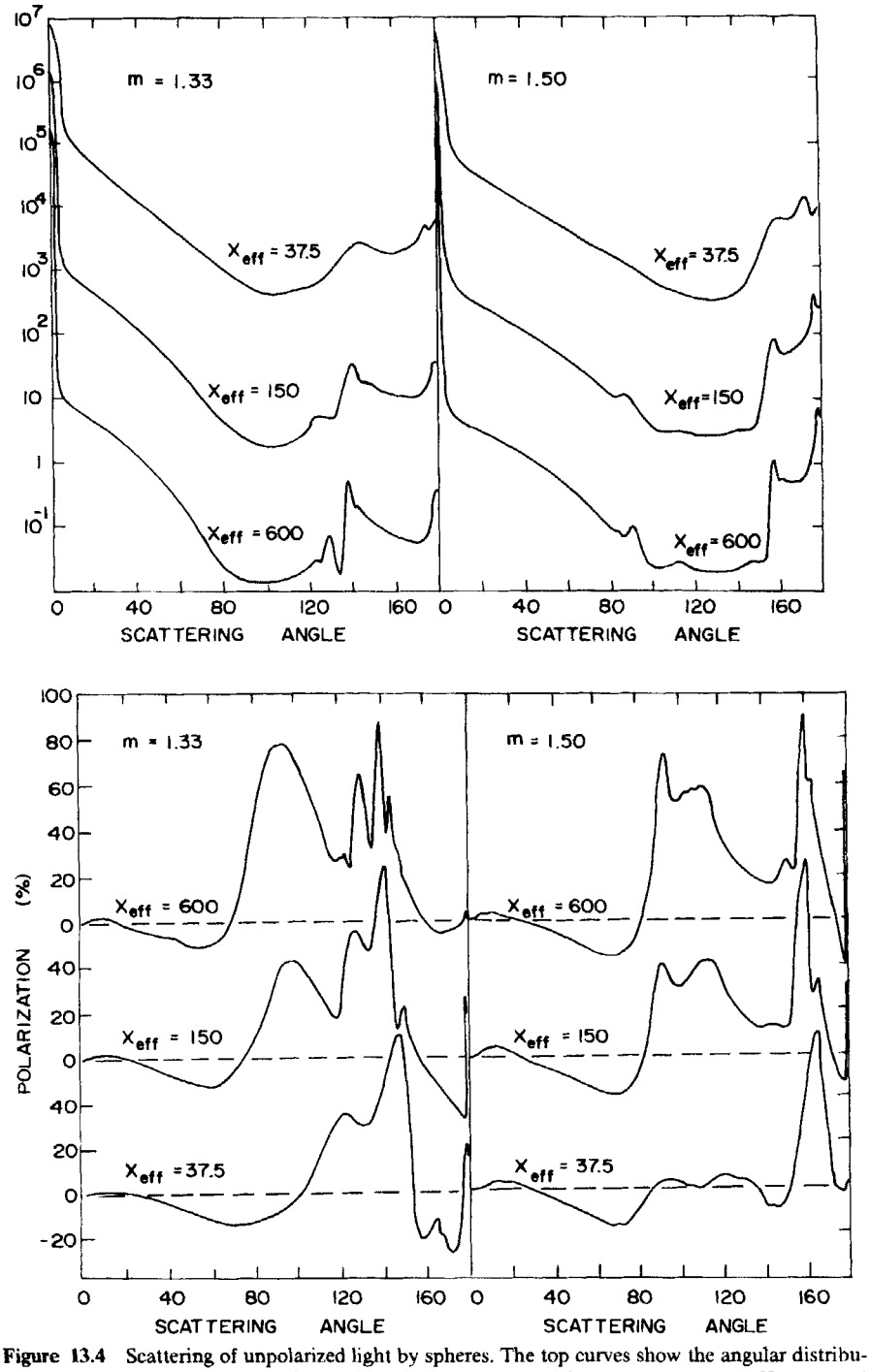

Figure 13.4 Scattering of unpolarized light by spheres. The top curves show the angular distribution of the scattered light and the bottom curves its degree of polarization. From Hansen and Travis (1974); copyright © 1974 by D. Reidel Publishing Company, Dordrecht, Holland.

and secondary ($\theta \simeq 129°$) rainbows, which may be attributed to one and two internal reflections, respectively, in a water droplet (see Section 7.2). Geometrical optics accounts well for the positions of the rainbows, which are rather insensitive to size for the larger droplets. The rainbow features are also prominent in the polarization curves.

Note the sharp increase in scattering near the backward direction, particularly for the largest spheres; this is the origin of the *glory*, one of the more spectacular natural phenomena. Observant passengers in airplanes flying above clouds may see the glory, a series of colored rings, around the shadow of the airplane. Unlike the rainbow the glory is not easy to explain, other than to say that it is a consequence of all the thousands of terms in the scattering series, a correct but unsatisfying statement. After all, the same statement could be made about the rainbow, which nevertheless has a simple physical explanation. A similar explanation of the glory, universally understood and accepted, has not yet been achieved, although there have been several admirable attempts toward this end, particularly recently. Rather than enter into a protracted digression on this interesting topic, we refer the reader to several relevant papers: those by van de Hulst (1947), Bryant and Cox (1966), Khare and Nussenzveig (1977), and Nussenzveig (1979).

13.2 TECHNIQUES OF MEASUREMENT AND PARTICLE PRODUCTION

Until about 10 years ago angular scattering measurements at visible wavelengths were limited to collections of *many* particles, either natural dispersions as in the atmosphere or those generated in the laboratory. With the advent of high-power lasers it has become feasible to measure light scattering by *single* particles. There are good reasons for measuring scattering by both single and many particles.

Most angular scattering measurements have been made at visible and near-ultraviolet wavelengths where detectors (primarily the photomultiplier tube) are sensitive, sources are intense, and good polarizing filters and other optical elements are readily available. These advantages of visible light diminish when we turn to other wavelength regions, although there is no lack of interest in them. The other principal wavelength region in which laboratory studies of angular scattering have been made is the microwave. As with extinction (see Chapter 11), scattering by single nonspherical and inhomogeneous particles in various orientations can be studied.

13.2.1 POLAR NEPHELOMETERS

An instrument for angular light scattering measurements is often called a *nephelometer*, from the Greek work *nephele* for cloud. To be more precise, the instrument shown schematically in Fig. 13.5 is a *polar* nephelometer, so named because of its angular detection capability. Its essential elements are a col-

limated light source and an arm that can be rotated about the sample (scattering cell); mounted on the arm is a detector system, which includes optical elements to collect light scattered within a small solid angle. The nephelometer shown in Fig. 13.5 is somewhat idealized, and each part of the instrument may be more complicated; descriptions of actual nephelometers are given, for example, by Stacey (1956), Pritchard and Elliot (1960), Holland and Gagne (1970), and Hunt and Huffman (1973).

The light source may be a lamp (tungsten–halogen, high-pressure mercury or xenon) with suitable collimators or, alternatively, a laser. Although lasers are easy to use and have seen wide use since their commercialization, it should not be assumed that a laser is always the best source; it certainly is not the most economical. A 300- to 500-watt tungsten–halogen lamp for home slide projectors is inexpensive and available at most photography shops; although only a small fraction of the rated power is available as visible light, the cost of a lamp is only a small fraction of that of a 1-watt continuous wave (CW) laser! Particularly for the study of collections of particles, where neither small beam size nor a high degree of monochromaticity is required, the tungsten–halogen lamp should be considered. In studies of scattering by a single particle, a laser is usually the best source.

The telescope on the detector arm, consisting of a lens followed by an aperture, limits the angular acceptance of the detector; this is accomplished at the expense of less detection sensitivity. The various factors determining resolving power and sensitivity are discussed by Pritchard and Elliot (1960). Intersection of the incident beam with the detector field of view determines the scattering volume (illuminated volume), which consequently changes with angle; therefore, the measured signal must be corrected by the multiplicative factor $\sin\theta$. It is not possible to make measurements at scattering angles near

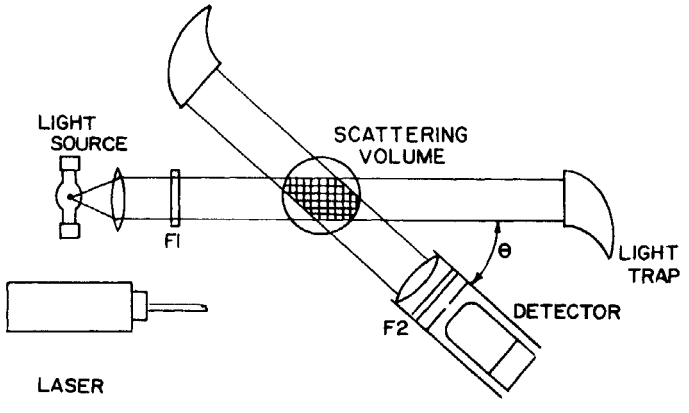

Figure 13.5 Schematic diagram of a polar nephelometer for measuring angular scattering. F1 and F2 are possible polarizing filters.

180° with conventional nephelometers because the arm interferes with the incident beam. Scattering at large angles is important, however, and this frequently requires that modifications be made so that these angles are accessible to measurement.

13.2.2 Absolute and Relative Measurements

Angular light scattering measurements are sometimes classified as either *absolute* or *relative*. In an absolute measurement I_s/I_i, which is directly related to the differential scattering cross section (13.2), is determined; in a relative measurement the irradiance is referred to some arbitrary scattering angle, say 10°, so that (assuming azimuthal symmetry)

$$\frac{I_s(\theta)}{I_s(10°)} = \frac{I_s(\theta)/I_i}{I_s(10°)/I_i} = \frac{dC_{\text{sca}}(\theta)/d\Omega}{dC_{\text{sca}}(10°)/d\Omega}.$$

Relative measurements are considerably easier to make and are the type most commonly reported. However, absolute measurements are of importance, for example, in comparing measured scattering cross sections of nonspherical particles with calculations for equivalent spheres. Note that "absolute" as we are using the term here means that scattering is not normalized to some arbitrary reference angle; it does not mean that absolute *irradiances* are measured, as with calibrated detectors. In both "relative" and "absolute" measurements, it is relative (i.e., dimensionless) *irradiances* that are determined.

Absolute measurements can be made by swinging the detector arm from 0° to θ, thereby obtaining I_i and $I_s(\theta)$; easy to say but less easily done: I_i may be thousands of times greater than I_s, and appreciable errors are likely because of the lack of detector linearity over such a range. One method for overcoming this is to attenuate I_i with neutral density filters to a level comparable with I_s; if the optical density is known, the unattenuated incident irradiance can be determined. Another technique is to use a diffusing surface, such as opal or MgO-smoked glass, in the incident beam to scatter light uniformly in all directions. Nonuniform illumination of the photocathode, arising from nonuniform illumination of the scattering volume, may also be a problem. Pritchard and Elliot (1960) and Holland and Gagne (1970) calibrated their instruments to account for these and other effects by moving a calibrated diffusing plate through the scattering volume and integrating the measured signal over the traverse for each angle and for all filter combinations. Perhaps the simplest technique is to use spheres (e.g., polystyrene) with known properties—concentration, size distribution, and refractive index—together with Mie calculations. For a given light source and optical elements such as filters, the detector signal D_r is measured with the reference sample in the scattering cell

$$D_r = KI_s = K\frac{I_i}{r^2}\left(\frac{dC_{\text{sca}}}{d\Omega}\right)_r,$$

where K is a dustbin (angle dependent) into which we deposit all our ignorance about instrument calibration factors. Under the same conditions another angular scan is made of the detector signal D with the "unknown" sample in the scattering cell

$$D = K\frac{I_i}{r^2}\frac{dC_{\text{sca}}}{d\Omega}.$$

$dC_{\text{sca}}/d\Omega$ is determined from the measured ratio of signals and $(dC_{\text{sca}}/d\Omega)_r$ calculated from Mie theory for the reference sample:

$$\frac{dC_{\text{sca}}}{d\Omega} = \frac{D}{D_r}\left(\frac{dC_{\text{sca}}}{d\Omega}\right)_r.$$

This technique is quite adaptable to instruments under the control of a microcomputer: the reference signal as well as calculated differential scattering cross sections are stored in the computer memory for a set of scattering angles; as the data scan proceeds the digital signal at each angle is divided by the reference signal and multiplied by the reference differential scattering cross section to give the absolute differential scattering cross section of the sample.

Because of the small amount of light scattered by dilute suspensions of particles it is necessary to carefully exclude extraneous light from the detector. Such light may originate from the surroundings (ambient light) or within the instrument itself. To exclude ambient light, measurements can be made in a darkroom; or the entire nephelometer can be enclosed in a dark box; or the scattering cell can be enclosed. The last option complicates the instrument by requiring a rotating light-tight aperture for the detector arm. Another possibility is to selectively reject the ambient light either with a light chopper and lock-in amplifier tuned to the chopper frequency or with a filter in the detector arm at the frequency of the source if it is nearly monochromatic. To exclude extraneous light originating from within the detector, light traps are used to stop the incident beam and as a backdrop for the detector (Fig. 13.5). Similarly, careful attention must be given to the design of the scattering cell, which may reflect forward-scattered light back into the detector. This is a particularly serious problem in the backscattering direction for large particles: even a very small amount of specular reflection from the scattering cell can easily dominate over scattering by the sample. Design of scattering cells becomes even more difficult for measurements of small amounts of circular polarization: strain-induced birefringence can give rise to appreciable errors.

13.2.3 Particle Production

Not only a nephelometer is needed to systematically study light scattering in the laboratory but also means for producing particles of known composition,

size distribution, and shape. A very useful device, therefore, would be a "magic particle maker" having a set of dials with which to specify the type of distribution and its parameters (mean size and width), chemical composition (to set the optical constants), and shape. When set for particle shape "sphere," for example, such a device used in conjunction with a calibrated nephelometer could give data similar to the curves of Figs. 13.1–13.3 calculated from Mie theory. Unfortunately, even for spheres, the simplest shape, such a magic box is not available. The experimenter who wishes to change a single parameter, such as mean size or refractive index, may have to work for several years to develop a different method of particle production; his theoretical counterpart need only change one number at a computer terminal! Thus, making well-defined collections of particles is a difficult task which has been undertaken in many laboratories for a long time. Only a few selected examples are given here.

For production of highly monodisperse aerosols, the Sinclair–LaMer generator (described by Kerker, 1969, p. 319) has often been used with success. Liquid droplets of controlled size in the approximate range 0.01–1 μm can be produced by condensing vapor onto nuclei created for the purpose. Careful control of temperature and temperature gradient permits the production of liquid aerosols with fractional standard deviations in particle radius of about 0.1–0.2. Various nebulizers have been used to generate liquid droplets which may be dried to yield particles of soluble solids. Size distributions from conventional nebulizers are often quite broad. An ultrasonic nebulizer, however, can give narrow distributions: the ultrasonic transducer excites surface waves in the liquid which can be driven to crest and break above the surface, releasing droplets of similar size at each crest (Lobdell, 1968); fractional standard deviation in size is about 0.3. Changing the frequency by using different transducers or higher harmonics enables droplet size to be varied. A vibrating orifice has been used to generate even narrower droplet size distributions (Bergland and Liu, 1973; Pinnick et al., 1973). A liquid is forced at high pressure through a small orifice. The orifice is driven into oscillation by an ultrasonic transducer, causing the emerging liquid to break off into droplets with size determined by the properties of the liquid, the applied pressure, the orifice size, and the vibration frequency. Relative size deviation is typically a few percent.

Liquid droplets with a dissolved component can be dried to leave a residue of solid aerosol particles with a size distribution similar to that of the parent liquid aerosol. Irregular solid particles have been produced beginning with droplets from an ultrasonic nebulizer (Perry et al., 1978) and droplets from a vibrating orifice (Pinnick et al., 1973; Pinnick et al., 1976; Pinnick and Auvermann, 1979). It is also possible to make aerosol particles that are not soluble in common liquids by means of chemical reactions in a flame. For example, following Nielsen et al. (1963) we have produced α-Fe_2O_3 (hematite) particles by nebulizing an aqueous solution of $FeCl_3$ and passing the resulting droplets into an air–hydrogen flame; α-Fe_2O_3 particles, with a mean size and standard deviation calculable from the original droplet size distribution, are

formed by the reaction

$$2FeCl_3 + 3H_2O \underset{\text{flame}}{\rightarrow} Fe_2O_3 + 6HCl.$$

The vibrating orifice method for producing monodisperse liquid aerosols, combined with drying or chemical reaction in a flame, comes about as close to being a magic particle maker as any technique we are aware of.

13.3 MEASUREMENTS ON SINGLE PARTICLES

In 1961, before lasers were a common laboratory instrument, Gucker and Egan published angular light-scattering measurements for single isolated particles. Since the advent of high-power collimated lasers many measurements on single particles have been published, particularly in the last decade, and instrument designs have proliferated. To successfully obtain angular light scattering information from single particles it is usually necessary to take one of two approaches: stably suspend the particles and use a conventional "take-your-time" nephelometer such as the one in Fig. 13.5, or make rapid measurements on single particles in flow. We shall discuss each of these in turn.

13.3.1 Particle Suspension Methods

There are several methods for levitating single particles. One of them uses a modified Millikan oil-drop apparatus in which the particle is charged and balanced against gravity by an electric field between parallel plates. To stabilize the particle laterally the electric field is deformed by a charged needle; an electronic servomechanism maintains the applied voltage at a level necessary to ensure vertical stability. This technique is described by Wyatt and Phillips (1972); it has been used for measurements on polystyrene spheres (Phillips et al., 1970), bacteria (Wyatt and Phillips, 1972), NaCl and NaCl–H_2O particles (Tang and Munkelwitz, 1978), and to determine diffusion coefficients (Davis and Ray, 1977). Particles suspended by electrostatic levitation tend to tumble randomly; this is an advantage in studies of scattering averaged over all particle orientations, but a disadvantage if one is interested in oriented particles.

A vertical laser beam has been used by Ashkin (1970) and Ashkin and Dziedzic (1971) to levitate weakly absorbing spherical particles by radiation pressure. Lateral stability results from the dominance of refracted over reflected components of the scattered light (see Table 7.1). Unequal reflection on opposite sides of the particle, which is caused by beam nonuniformity, produces a net force that drives the particle toward lower light levels; this instability is countered by refraction, which produces a reaction that drives the particle toward higher light levels. The particle is thus laterally stabilized in the most intense part of the beam. Laser levitation has the disadvantage that it

cannot be used with strongly absorbing particles, which are likely to vaporize in beams sufficiently powerful for levitation.

Perhaps the simplest, but least used method for supporting single particles is to attach them to very fine fibers such as drawn glass fibers or spider threads (Saunders, 1970, 1980). The fiber diameter can be made small compared with particles larger than about 1 μm. Furthermore, the characteristics of scattering by long cylinders (see Section 8.4, particularly Fig. 8.5) can be used to advantage: scattering by fibers oblique to the scattering plane is confined to directions only one or two of which lie in this plane. This simple method provides a means for fixing the orientation of a particle; its disadvantages are the need to consider scattering by the support fiber and the possibility of electromagnetic interaction between the fiber and the particle.

13.3.2 Rapid Light Scattering Measurements

Rather than suspend a particle in the scattering volume for a time sufficient to make a scan with a conventional nephelometer, scattering data can be recorded rapidly during the short time it takes a particle to transit the scattering volume. This can be done in two ways: (1) with a *rotating* detector or aperture (or both), or (2) with an array of *fixed* detectors.

Marshall et al. (1976) used an annular segment of an ellipsoidal mirror to direct light scattered by a particle at one focus to a detector fixed at the other focus; an aperture (5°) rotating at 3000 rpm then gives a 360° scan in 20 msec. Morris et al. (1979) mounted a detector on a turntable that rotates at 1 Hz; in 1 sec this gives a scan from 0 to 180° and from 180 to 360°; these scans are not necessarily identical. There are at least two reasons for making 360° scans instead of the usual 180° scans: single particles (other than spheres) are likely to be azimuthally asymmetric; and such scans show instrument misalignment.

Fixed detector arrays were devised by Diehl et al. (1979) and by Bartholdi et al. (1980) to measure scattering by single particles. The former authors mounted detectors at $\pm 45°$, $\pm 90°$, $\pm 135°$, combinations of either two or three of which sampled scattered light at 16.7-msec intervals (60-Hz sampling rate). The instrument of Bartholdi et al. has an annular segment of an ellipsoidal reflector to focus scattered light onto a circular array of 60 photodiode detectors. This instrument was designed for applications in which biological cells flow in single file (at flow rates of up to 1000 particles per second) through the scattering volume; by analyzing the scattered light, cells from heterogeneous populations can be identified and possibly separated downstream.

13.3.3 Microwave Analog Scattering

Microwave scattering is an important analog technique for investigating scattering of visible light by single nonspherical particles. Because of the ratio of about 10^5 between microwave and visible wavelengths, arbitrarily oriented

particles of many shapes and with microwave size parameters of less than 1 can be readily fashioned (e.g., by machining); materials can be chosen with microwave optical constants closely matching those at visible wavelengths for particles of interest. Microwave extinction ($\theta = 0°$) has already been discussed in Section 11.7; to adapt the instrument shown in Fig. 11.22 to angular scattering measurements, the receiving antenna need only be mounted so that it can move about the particle. Extraneous radiation reflected from walls, floor, and ceiling is usually eliminated by the liberal use of absorbing material.

Materials with microwave optical constants similar to those of common solids in the visible have been made from plastics of varying density; an absorber, such as fine carbon dust, can be added to increase the imaginary part of the refractive index. For example, acrylic plastic (Dupont trade name, Lucite) has a microwave refractive index of about 1.6, which is similar to that of some silicate materials in the visible. Polystyrene beads impregnated with a volatile material can be expanded by heating to form a foam with an effective refractive index which depends on its density. In this way a material with optical constants similar to those of ice or water at visible wavelengths can be made. The microwave optical constants of such composite media are determined by techniques similar to those that are used for homogeneous media (Chapter 2); the fact that these optical constants can be used in Mie calculations for homogeneous spheres which agree with experiment is a partial justification for treating some composite media as homogeneous with effective refractive indices, although this does not necessarily follow for all combinations of materials (see Section 8.5 for a discussion of theories of optical constants for inhomogeneous media). There are practical limits to the range of microwave optical constants obtainable with common materials: for example, optical constants close to those that give strong shape-dependent scattering and absorption (see Chapter 12), such as $n = 0$ and $k = \sqrt{2}$, would probably be difficult to obtain.

Microwave angular scattering measurements for incident light polarized parallel and perpendicular to the scattering plane have been made by Zerull and Giese (1974) and by Zerull et al. (1977, 1980) for particles of various shapes, including spheres, spheres with roughened surfaces, cubes, octahedrons, irregular particles with both convex and concave surfaces, and "fluffy" particles consisting of loose aggregates of smaller compact particles; n was mostly in the range from about 1.5 to 1.7 and k between about 0.005 and 0.015. Greenberg et al. (1961) investigated scattering by spheroids and finite cylinders; they chose materials with microwave optical constants similar to those of water and silicate materials at visible wavelengths.

The microwave analog technique has the great advantage that scattering by single particles of any shape and orientation can be studied with relative ease; within limits, the optical constants can also be varied arbitrarily by using composite media. Therefore, microwave experiments should be the best test of theories of scattering by irregular particles, such as those discussed in Section 8.6. For collections of randomly oriented particles, however, microwave mea-

surements can be quite laborious: measurements for many orientations must be made at each scattering angle and for many particles. Examples of angular scattering of microwave radiation are given in the following section.

13.4 SOME THEORETICAL AND EXPERIMENTAL RESULTS

Measurements of angular scattering by spheres agree well with Mie calculations, both for single spheres (Marshall et al., 1976; Bartholdi et al., 1980; Phillips et al., 1970) and for monodisperse collections of spheres (e.g., Pinnick et al., 1976). Sphere measurements are now used primarily to check instrument operation and calibration or to infer some physical property from accurate determinations of size and refractive index (Davis and Ray, 1977, for example). The present thrust in light scattering, both theoretical and experimental, is toward a better understanding of nonspherical particles, although the standard of comparison is likely to be Mie calculations for equivalent spheres.

Numerical approximation techniques can now handle almost any nonspherical and inhomogeneous particle, but the computational demands are high, especially when a distribution of shapes, sizes, and orientations must be considered. An additional complication is that scattering by nonspherical particles may depend on the azimuthal angle ϕ as well as the scattering angle θ, which makes scattering diagrams less easy to display.

13.4.1 Scattering by Spheroids

A spheroid is perhaps the simplest (finite) nonspherical particle. Many approximate treatments of spheroids, valid for certain limiting cases, have been given (see e.g., Section 5.3). Two approaches to the problem of scattering by spheroids of arbitrary shape and composition, which have been taken in recent years, are (1) constructing separable solutions to the scalar wave equation in spheroidal coordinates and expanding the fields in vector spherical harmonics in a manner similar to that for spheres (Section 4.1), and (2) using the T-matrix method of Waterman (1965, 1971) (Section 8.6). The former approach was initiated by Asano and Yamamoto (1975); the latter adopted by Barber and Yeh (1975). Both of these methods are exact. Scattering by spheroids has also been investigated within the framework of various approximate methods (Latimer et al., 1978).

Calculated scattering of unpolarized light by spheroids is shown in Figs. 13.6 and 13.7. In the first figure polar scattering diagrams of Latimer et al. (1978) are displayed for equal-volume spheroids (1 μm^3)—sphere, prolate, oblate—with symmetry axes parallel to the scattering plane and in various orientations relative to the incident beam; the refractive index $m = 1.05$, which approximately corresponds to that of biological cells in water at visible wavelengths, reflects the authors' interest in particles of biological origin. Scattering diagrams from Asano (1979) are shown in Fig. 13.7 for two different

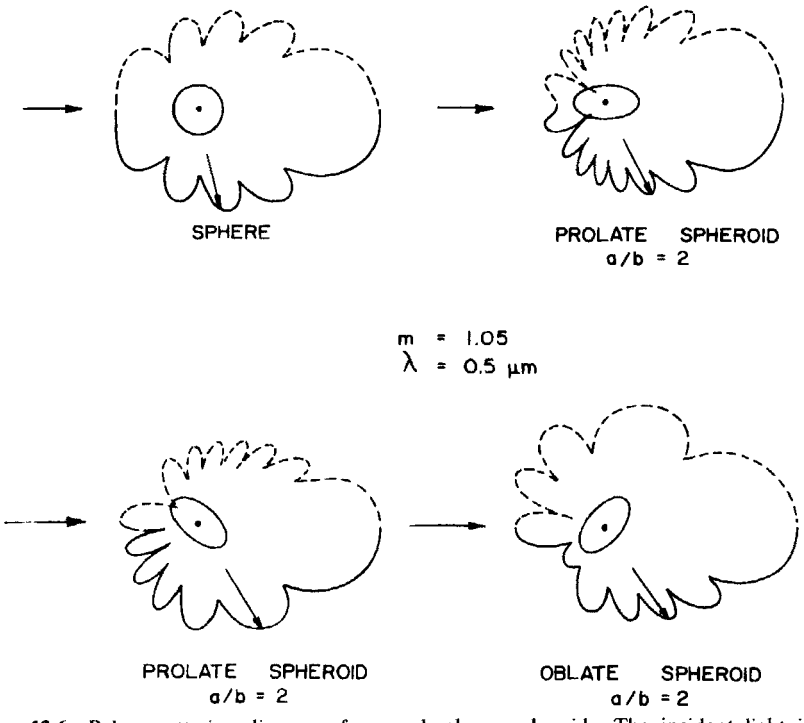

Figure 13.6 Polar scattering diagrams for equal-volume spheroids. The incident light is unpolarized. From Latimer et al. (1978).

orientations of a spheroid with axial ratio 5.0 and refractive index 1.5; the symmetry axis is again parallel to the scattering plane.

Note first that spheroids oriented with their symmetry axes oblique to the incident beam scatter asymmetrically about the forward direction; this is more evident in the polar plots of Fig. 13.6. Latimer et al. pointed out that there tend to be more lobes in the scattering diagram near directions toward which the particle presents a large width than near directions for which the projected width is smaller; this is somewhat analogous to scattering by spheres: the larger the sphere, the more lobes there are. They also concluded that for sufficiently large particles (radius of equal volume sphere greater than about 1 μm), small-angle (1.5°) scattering is strongly dependent on shape and orientation. In general, the larger the spheroid, the greater the number of lobes in the scattering diagram and the more it is peaked in the forward direction. Note in Fig. 13.7 that forward scattering by a prolate spheroid is greater when its axis is parallel (0°) than when it is oblique (45°) to the incident beam even though it presents a smaller area to the beam in the parallel orientation. The effect of increasing absorption (not shown in the figure but discussed by Asano) is to dampen oscillations in the scattering diagram.

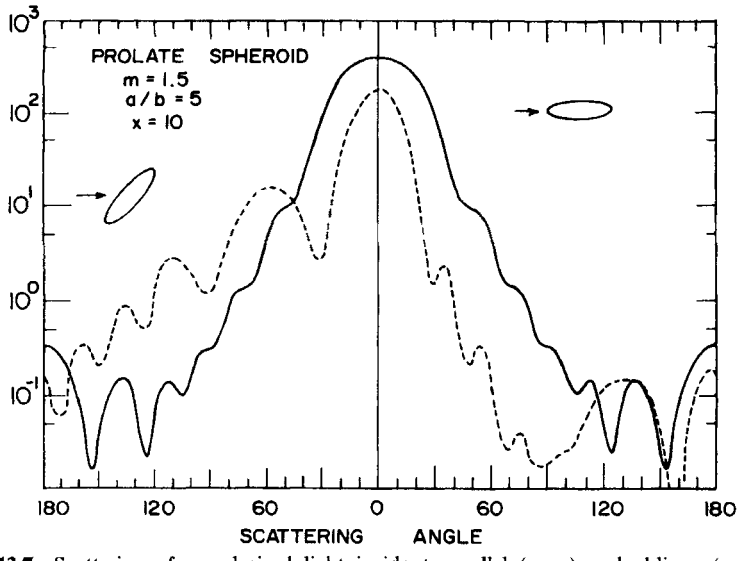

Figure 13.7 Scattering of unpolarized light incident parallel (——) and oblique (---) to the symmetry axis of a spheroid. From Asano (1979).

Asano also gives scattering diagrams for a large, slender prolate spheroid illuminated obliquely (45°), but in scattering planes that do not contain the symmetry axis; scattering resembles that by infinite circular cylinders (Section 8.4). Scattering by single coated spheroids is discussed by Wang and Barber (1979).

Scattering depends on azimuthal angle for arbitrarily oriented spheroids but not for collections of randomly oriented spheroids. Therefore, if theory is to be compared with measurements either on collections of randomly oriented particles or on single particles randomized by tumbling, calculations must be done for many orientations. This has not been done in most calculations. Exceptions are the work of Wang et al. (1979) on coated as well as homogeneous spheroids and that of Asano and Sato (1980). Because of the range of sizes and refractive indices considered, the latter paper is particularly valuable for comparing theory with experimental results; the physical mechanisms responsible for departures from scattering by spheres are also discussed at length by Asano and Sato.

13.4.2 Scattering by Collections of Particles

Several examples of scattering by spherical and by nonspherical particles are collected in Fig. 13.8: calculations for randomly oriented prolate and oblate spheroids; measured scattering of microwave radiation by a polydispersion of nonspherical particles; and measured scattering of visible light by irregular

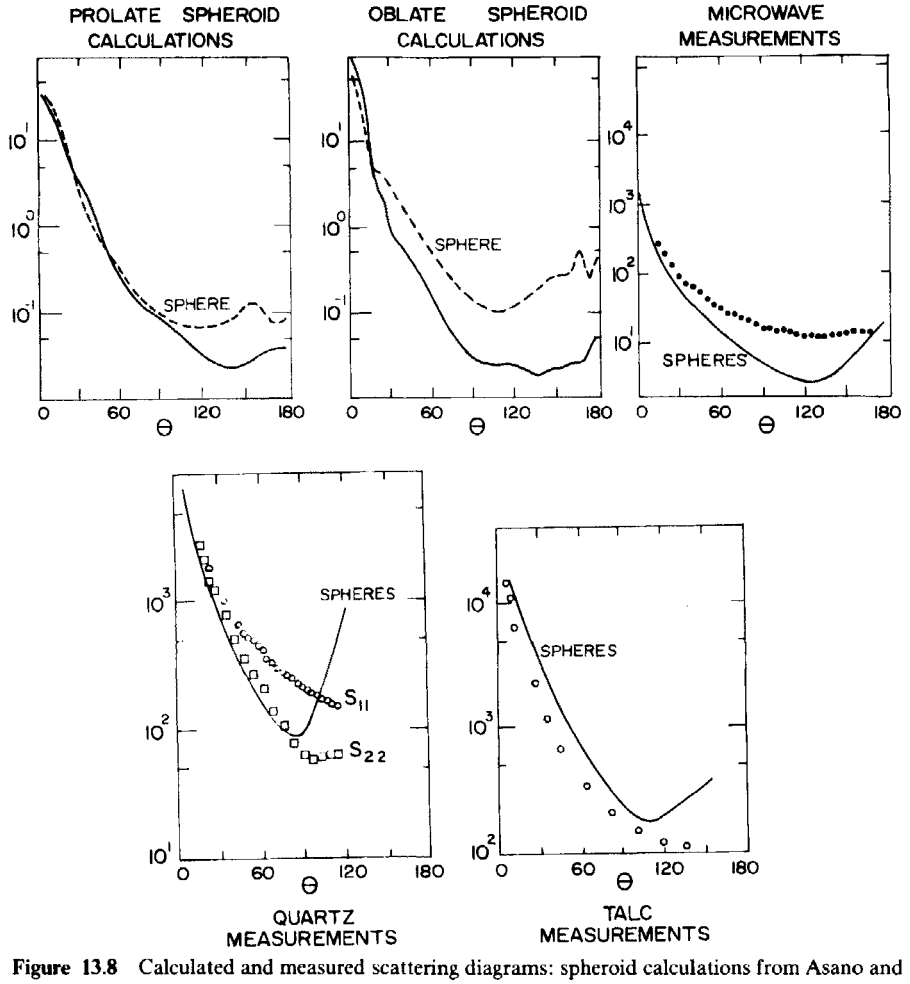

Figure 13.8 Calculated and measured scattering diagrams: spheroid calculations from Asano and Sato (1980); microwave measurements from Zerull et al. (1980); quartz measurements from Holland and Gagne (1970); and talc measurements from Holland and Draper (1967).

quartz and by talc particles. Accompanying each of these are calculations for equivalent spheres. The meaning of equivalent, as well as size parameters and refractive indices, is given in the papers (cited in the figure caption) from which these curves were taken (redrafted for uniformity).

There are both similarities and differences between scattering by spherical and by nonspherical particles. Near the forward direction, where scattering may be associated primarily with diffraction, external reflection, and twice-refracted transmission (Hodkinson and Greenleaves, 1963), nonspherical particles scatter similarly to area-equivalent spheres, in general. Forward scattering by large particles is dominated by diffraction, which depends on particle

area and is independent of refractive index; for this reason, forward scattering may be used to size nonspherical particles with unknown optical properties. Features in scattering diagrams for spheres, such as rainbows, are not exhibited by nonspherical particles. In directions greater than about 90°, scattering diagrams for nonspherical particles tend to be flatter than those for spheres; in particular, scattering does not increase sharply near the back direction (i.e., glories are not associated with nonspherical particles). It is difficult to generalize about differences between scattering by nonspherical and equivalent spherical particles at intermediate scattering angles (in the range 45–135°, say), which may reflect the absence of a general trend: equivalent spheres scatter less at these angles than irregular quartz particles and cubes but more than talc particles and spheroids. These differences also appear in calculated asymmetry parameters. Asano and Sato (1980) calculated asymmetry parameters for randomly oriented spheroids which were greater than those for equivalent spheres; in contrast, Pollack and Cuzzi (1980) calculated asymmetry parameters for various nonspherical particles which were less. Therefore, it is not possible to state categorically that nonspherical particles are either more or less backscattering than equivalent spheres.

13.4.3 Polarization

Calculated and measured values of $P = -S_{12}/S_{11}$, the degree of linear polarization, for several nonspherical particles are shown in Fig. 13.9. The prolate and oblate spheroids, cubes, and irregular quartz particles have made their appearance already (Fig. 13.8); a new addition is NaCl cubes. Also shown are calculations for equivalent spheres.

There are marked differences between the polarization diagrams for spherical and nonspherical particles; moreover, a few generalizations appear to be possible. First, polarization diagrams for nonspherical particles do not have features near the rainbow angles (or their precursors for smaller particles) for equivalent spheres. Second, polarization tends to be positive over a wide range of angles for nonspherical particles. On the basis of extensive calculations for randomly oriented prolate spheroids with axial ratio 2, refractive index 1.44, and size parameters up to about 15, Asano and Sato (1980) concluded that the linear polarization of light scattered by nonspherical particles, in contrast with spheres, tends to be positive at middle scattering angles. Perry et al. (1978) measured scattering by nearly cubical NaCl particles of various sizes and found good agreement with calculations for small spheres ($x < 4$) but poor agreement for larger spheres (Fig. 13.9). They also found good agreement for all sizes up to $x = 12.4$ for rounded, but not spherical, ammonium sulfate particles. Similar positive polarization was observed in scattering by plate-like ice crystals (Sassen and Liou, 1979). Thus, for a variety of nonspherical particles, there appears to be a trend toward polarization opposite to that for spheres. Geometrical optics predicts that light externally and internally reflected by a sphere will contribute positively to linear polarization; note, for

example, that the polarization is positive at the primary and secondary rainbow angles (Fig. 13.4), which are associated with rays internally reflected once and twice, respectively. Shape irregularities apparently distribute the positive polarization attributed to internal reflections over a larger range of angles (see, e.g., Coffeen, 1969).

Also shown in all but one of the examples of Fig. 13.9 is the normalized matrix element S_{22}/S_{11}, which is unity for all collections of spheres. Thus, the

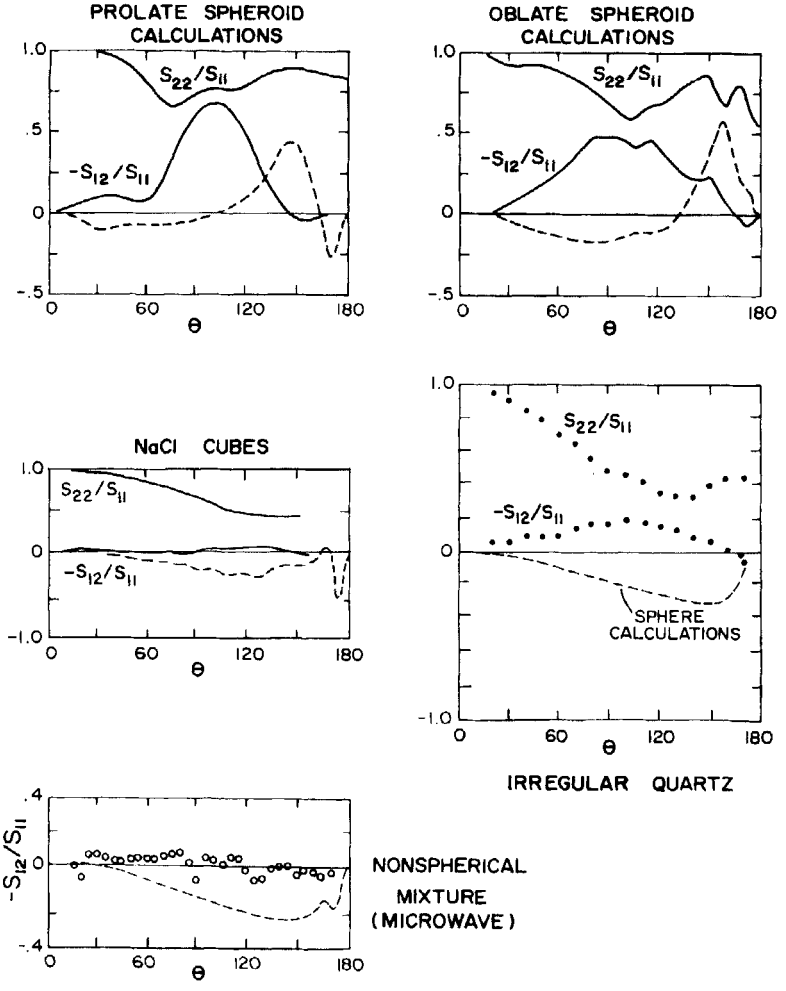

Figure 13.9 Calculations and measurements of $-S_{12}/S_{11}$ (linear polarization) and S_{22}/S_{11}: spheroid calculations from Asano and Sato (1980); NaCl measurements from Perry et al. (1978); quartz measurements from Holland and Gagne (1970) (calculated using their measurements of unnormalized matrix elements); and microwave measurements from Zerull et al. (1980). Dashed curves are calculations for equivalent spheres.

departure of S_{22}/S_{11} from unity is a measure of nonsphericity; the difference

$$\Delta = 1 - \frac{S_{22}}{S_{11}}$$

is sometimes called the *depolarization ratio*. In Section 13.1, however, $\frac{1}{2}(S_{11} - S_{22})$, which is the same as Δ except for the normalization factor S_{11}, was called the *cross polarization*. If Δ is zero, then under the assumption that the scattering matrix has the form (13.21) there is no depolarization of incident light polarized either parallel or perpendicular to the scattering plane (i.e., the scattered light is 100% polarized). However, Δ is measured by inserting linear polarizers with orthogonal transmission axes—crossed polarizers—fore and aft of the scattering medium. Thus, the term "depolarization ratio" for Δ reflects its physical significance, whereas the term "cross polarization" reflects the method by which it is measured.

All the examples in Fig. 13.9 show S_{22} approaching S_{11} in the forward direction, but S_{22}/S_{11} deviates appreciably from unity at large angles. For example, S_{22}/S_{11} for the NaCl cubes is less than about 0.5 at scattering angles greater than 90°. Calculations for prolate spheroids yield an interesting result: the depolarization ratio for spheroids with axial ratio 2 is greater than that for more elongated spheroids with axial ratio 5.

13.4.4 Implications for the Inverse Scattering Problem

In attempts to invert scattering data to infer properties of particles in the atmosphere, in interstellar space, and in the laboratory, differences between scattering by spherical and nonspherical particles can lead to conclusions that are quantitatively as well as qualitatively incorrect. For example, a flat response for S_{11} in back directions could be mistaken as an effect of large absorption in spheres rather than nonsphericity in weakly absorbing particles. Large positive polarizations could suggest very small particles rather than larger nonspherical particles. On the other hand, deviations of S_{22}/S_{11} from unity could be valuable indicators of nonsphericity, which would then signal caution in analyzing and interpreting experimental results with Mie theory.

13.5 PARTICLE SIZING

Particle sizing by elastic light scattering has been used widely because it is nondestructive and may be done rapidly. Kerker (1969, Chap. 7) has discussed in detail several particle sizing methods, including those for collections of particles distributed in size. The difficulty of inverting measurements to obtain a size distribution increases with its width. This drawback has led to greater use of methods in which light scattered by particles flowing singly through the scattering volume is analyzed to infer sizes. Pulses of light scattered into a set of directions are detected and sorted electronically into bins according to height; the size distribution is determined from the pulse height histogram by

means of a calibration curve relating pulse height to particle size. Commercial instruments are now available for this purpose; they differ according to the directions for which scattered light is collected and the source of illumination, which can be a laser or focused light from an incandescent lamp.

The response R of a single-particle light scattering instrument is

$$R = \iint G \frac{dC_{sca}}{d\Omega} f \, d\lambda \, d\Omega;$$

G describes the illumination and collection geometry, f includes the source spectrum and spectral sensitivity of the photodetector, and the differential scattering cross section $dC_{sca}/d\Omega$ can be calculated from Mie theory if the particles are spheres. Response as a function of particle size for several commercial instruments has been published by various authors, including Cooke and Kerker (1975) and Pinnick and Auvermann (1979). Calculations for spheres by the latter authors are shown in Fig. 13.10; ripple and interference structure (see Chapters 4 and 11) are evident in the curves for the nonabsorbing spheres. These curves demonstrate some of the problems that must be faced in the design and use of particle sizing instruments. Because of the interference structure, response is a multivalued function of size: spheres of three different sizes can give the same response. This can be mitigated to some extent for certain kinds of aerosols by choosing the electronic discriminator setting to avoid regions of multivaluedness. If spheres of unknown or different refractive indices are to be sized, the variation of response with refractive index can be a problem.

Two instruments considered by Cooke and Kerker (1975) had single-valued response functions, presumably because of broad-band (white) light sources and large angular apertures for both incident and scattered light.

Calibration is invariably based on spheres, which means that an instrument can be used with confidence only for such particles. Of course, a response will duly be recorded if a nonspherical particle passes through the scattering volume. But what is the meaning of the "equivalent" radius corresponding to that response? Is it the radius of a sphere of equal cross-sectional area? Or equal surface area? Or equal volume? Or perhaps equal mean chord length? Answers to these questions depend on the particular instrument and nonspherical particle; comprehensive answers do not come easily because it is difficult to do calculations for nonspherical particles, even those of regular shape.

According to scalar diffraction theory (Section 4.4) the scattering amplitude in the forward direction is proportional to the cross-sectional area of the particle, regardless of its shape, and is independent of refractive index. To the extent that diffraction theory is a good approximation, therefore, the radius corresponding to the response of an instrument that collects light scattered near the forward direction by a nonspherical particle is that of a sphere with equal cross-sectional area. The larger the particle, however, the more the

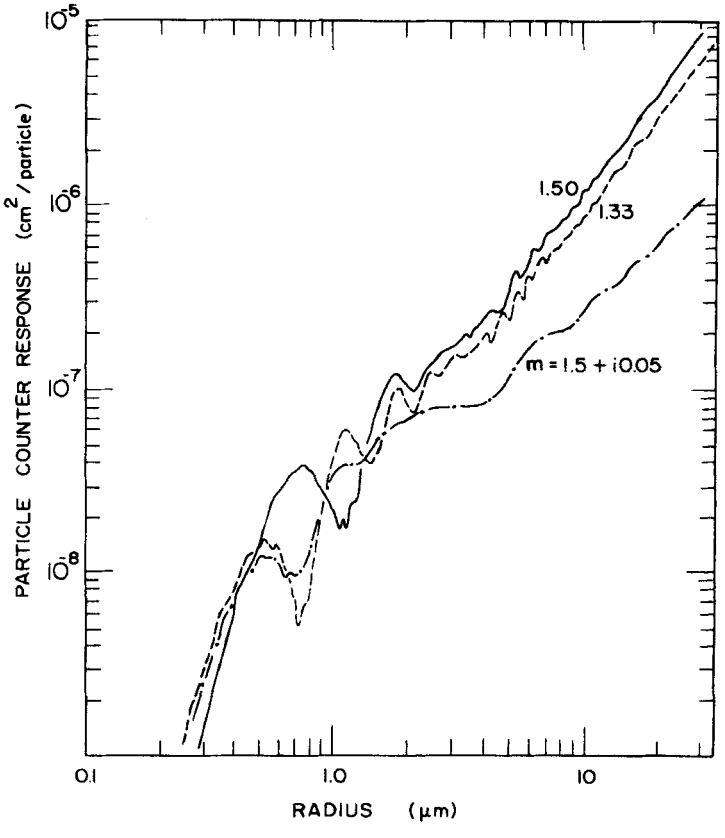

Figure 13.10 Response calculations for a particle counter that collects He–Ne laser light scattered between 4 and 22°. Reprinted with permission from R. G. Pinnick and J. J. Auvermann, *J. Aerosol Sci.*, **10** (1979), 55–74; copyright 1979, Pergamon Press, Ltd.

scattered light is peaked in the forward direction and the more difficult it is to discriminate between scattered and unscattered (incident) light. Nevertheless, the possible advantages of refractive index independence and insensitivity to shape make low-angle scattering an attractive method of particle sizing. Based on calculations of response functions for various instruments Heyder and Gebhart (1979) concluded that size distributions of particles with unknown refractive indices can be determined accurately by low-angle scattering of polychromatic light.

Experimental evaluation of various widely used commercial instruments has been undertaken by several investigators, including Liu et al. (1974), who used the vibrating orifice technique to generate spherical aerosols with narrow size distributions. Similarly, Pinnick and Auvermann (1979) generated droplets of a solution which were dried to make solid particles for evaluating the response of

certain instruments to nonspherical aerosols. It appears from these evaluations that, depending on the instrument, spherical particles in the size range between about 0.2 and 15 μm can be sized accurately by light scattering if their refractive index is known. If, however, the particles are nonspherical, or of unknown refractive index, or if the aerosol is composed of particles with different refractive indices, accurate sizing may be less attainable.

13.6 SCATTERING MATRIX SYMMETRY

All the information about angular scattering by a medium (a single particle or a collection of particles) is contained in the 16 elements of its scattering matrix. In many instances—media with rotational symmetry, for example—all the matrix elements are not independent, and higher symmetry often further reduces the number of independent, nonzero elements. Even without considering its explicit angular dependence, therefore, the *form* of the scattering matrix reflects general properties of the scattering medium. The two major treatments of scattering matrix symmetry, those of Perrin (1942) and van de Hulst (1957, Chap. 5), arrive at similar results but by somewhat different paths: van de Hulst begins with 2×2 amplitude scattering matrices for single particles and derives 4×4 scattering matrix symmetries under various assumptions about the distribution of particle orientation and shape; Perrin, however, considers the scattering matrix directly without going through the intermediate step of appealing to symmetries of the 2×2 matrices. Because 2×2 amplitude scattering matrices for single particles are conceptually simpler than 4×4 scattering matrices for collections of particles, our approach to scattering matrix symmetry follows that of van de Hulst.

The most general amplitude scattering matrix for a *single* particle

$$\begin{pmatrix} S_2(\theta, \phi) & S_3(\theta, \phi) \\ S_4(\theta, \phi) & S_1(\theta, \phi) \end{pmatrix} \tag{13.4}$$

contains eight parameters, the real and imaginary parts of each element, or equivalently, the amplitude and phase, which depend on the scattering angle θ and the azimuthal angle ϕ. Because only *relative* phases are physically significant, there are in fact only seven *independent* parameters in (13.4). The 4×4 scattering matrix corresponding to (13.4) follows from (3.16); although all of its 16 elements may be nonzero, only seven of them are independent. Thus, there are nine independent relations among the matrix elements; these were given by Abhyankar and Fymat (1969). However, the scattering matrix for a collection of *different* particles, different by virtue of orientation or shape or composition, is not so constrained: all of its 16 elements may be independent. Nevertheless, there is still a set of independent *inequalities* relating the matrix elements (Fry and Kattawar, 1981). For example, if the particles are spherical,

we have

$$S_{11}^2 \geqslant S_{12}^2 + S_{33}^2 + S_{34}^2.$$

Equality holds for a single sphere or a collection of identical spheres; inequality holds if they are distributed in size or composition. This inequality was used by Hunt and Huffman (1973), for example, as an indicator of dispersion in suspensions of spherical particles. It was pointed out by Fry and Kattawar (1981) that the inequalities they derived are useful consistency checks on measurements of all 16 scattering matrix elements.

In the following paragraphs we shall first discuss scattering matrices corresponding to specific particles for which analytical solutions to the scattering problem exist. Then, by appealing to very general symmetry relations, we shall obtain the form of scattering matrices without regard to the detailed nature of the particles.

13.6.1 Single-Particle Symmetries

We first point out a few scattering matrix symmetries for single particles based on results in previous chapters.

For spheres sufficiently small that Rayleigh theory (Chapter 5) is applicable, or for arbitrarily shaped particles that satisfy the requirements of the Rayleigh–Gans approximation (Chapter 6), incident light with electric field components parallel and perpendicular to the scattering plane may be scattered with different amplitudes; however, there is no phase shift between the two components. Hence, the amplitude scattering matrix has the form

$$\begin{pmatrix} FA_2 & 0 \\ 0 & FA_1 \end{pmatrix},$$

where F, the common factor, is complex, and A_1, A_2 are real. The corresponding scattering matrix is, from (3.16),

$$\begin{pmatrix} S_{11} & S_{12} & 0 & 0 \\ S_{12} & S_{11} & 0 & 0 \\ 0 & 0 & S_{33} & 0 \\ 0 & 0 & 0 & S_{33} \end{pmatrix}. \tag{13.5}$$

Note that the cross polarization is zero and incident unpolarized light does not acquire a degree of circular polarization upon scattering.

Both the amplitudes and relative phase of the field components parallel and perpendicular to the scattering plane can be changed upon scattering by a sphere of arbitrary size and composition. Symmetry, however, precludes any mechanism for transforming parallel to perpendicularly polarized light, and

vice versa. Thus, the cross polarization is zero, and the amplitude scattering matrix must have the form

$$\begin{pmatrix} S_2 & 0 \\ 0 & S_1 \end{pmatrix},$$

which leads to the 4 × 4 matrix

$$\begin{pmatrix} S_{11} & S_{12} & 0 & 0 \\ S_{12} & S_{11} & 0 & 0 \\ 0 & 0 & S_{33} & S_{34} \\ 0 & 0 & -S_{34} & S_{33} \end{pmatrix}. \tag{13.6}$$

The only difference between (13.6) and (13.5) is that for an arbitrary sphere the matrix element S_{34} does not, in general, vanish. The effect of this matrix element is the same as that of a retarder such as a quarter-wave plate: the phase of one orthogonal component of the incident light is retarded relative to the other, which gives a degree of circular polarization to the scattered light if the incident light is polarized obliquely to the scattering plane. A consequence of the zero off-diagonal elements of the amplitude scattering matrix is that S_{11} and S_{22} are equal as are S_{33} and S_{44}. The scattering matrix for a normally illuminated cylinder (Section 8.4) has the same symmetry as (13.6).

The off-diagonal elements of the amplitude scattering matrix for an optically active sphere (Section 8.3)

$$\begin{pmatrix} S_2 & S_3 \\ -S_3 & S_1 \end{pmatrix} \tag{13.7}$$

do not, in general, vanish; neither do those for an infinite cylinder illuminated at oblique incidence (Section 8.4). The 10-parameter scattering matrix corresponding to (13.7) is

$$\begin{pmatrix} S_{11} & S_{12} & S_{13} & S_{14} \\ S_{12} & S_{22} & S_{23} & S_{24} \\ -S_{13} & -S_{23} & S_{33} & S_{34} \\ S_{14} & S_{24} & -S_{34} & S_{44} \end{pmatrix}. \tag{13.8}$$

It is the off-diagonal elements of (13.7) that give rise to cross polarization ($S_{11} \neq S_{22}$) as well as the nonzero elements S_{13}, S_{14}, S_{23}, and S_{24} in (13.8). That S_3 and S_4 should be nonzero for optically active particles follows from elementary physical reasoning: optical rotatory power in a homogeneous medium causes the direction of vibration to be rotated upon transmission of linearly polarized light by the medium. However, optical activity of the bulk

parent material is merely sufficient, not necessary, for a particle to have nonzero cross polarization; for example, it is nonzero for isotropic, nonactive, elongated particles, such as prolate spheroids or circular cylinders, illuminated obliquely to their symmetry axes. The scattering matrices for an obliquely illuminated infinite circular cylinder are identical in form with those for an optically active sphere; it should be recalled, however, that the orthogonal basis vectors for specifying the incident electric field are parallel and perpendicular to the plane determined by the incident beam and the cylinder axis rather than by the incident beam and the scattering direction.

We have about exhausted possible scattering matrix symmetries obtained by appealing to approximate or exact solutions to specific scattering problems. But more can be said about particles, regardless of their shape, size, and composition, without explicit solutions in hand. The scattering matrix for a given particle implies those for particles obtained from this particle by the symmetry operations of rotation and reflection. We shall consider each of these symmetry operations in turn.

Consider an arbitrary particle illuminated by a plane wave *with unit amplitude* and linearly polarized along the direction $\hat{\mathbf{q}}$. The direction of propagation of this wave is specified by the unit vector $\hat{\mathbf{e}}_i$ and that of the scattered wave—that is, the direction of observation—by $\hat{\mathbf{e}}_s$. We denote by $\mathbf{A}(\hat{\mathbf{q}}; \hat{\mathbf{e}}_i, \hat{\mathbf{e}}_s)$ the amplitude of the scattered wave, where $\hat{\mathbf{e}}_i \cdot \hat{\mathbf{q}} = 0$ and $\hat{\mathbf{e}}_s \cdot \mathbf{A}(\hat{\mathbf{q}}; \hat{\mathbf{e}}_i, \hat{\mathbf{e}}_s) = 0$. The Maxwell equations (2.1)–(2.4) are invariant under time reversal: they have the same form if t is replaced by $-t$, $\mathbf{H}$ by $-\mathbf{H}$, and $\mathbf{J}_F$ by $-\mathbf{J}_F$. Reversal in time implies that an incident photon becomes a scattered photon and conversely. Or, stated another way, if a plane wave incident on a particle gives rise to a scattered outgoing spherical wave, then an incoming spherical wave will give rise to a scattered outgoing plane wave. This is not quite sufficient for our purposes because we are interested in scattering of plane waves, not spherical waves. However, if only the *directions* of incident and scattered waves are interchanged, then the amplitudes are connected by a *reciprocity relation* proved by Saxon (1955ab).

$$\hat{\mathbf{q}}' \cdot \mathbf{A}(\hat{\mathbf{q}}; \hat{\mathbf{e}}_i, \hat{\mathbf{e}}_s) = \hat{\mathbf{q}} \cdot \mathbf{A}(\hat{\mathbf{q}}'; -\hat{\mathbf{e}}_s, -\hat{\mathbf{e}}_i), \tag{13.9}$$

where $\hat{\mathbf{q}}' \cdot \hat{\mathbf{e}}_s = 0$ and $\hat{\mathbf{e}}_i \cdot \mathbf{A}(\hat{\mathbf{q}}'; -\hat{\mathbf{e}}_s, -\hat{\mathbf{e}}_i) = 0$. This reciprocity relation is the key to obtaining the form of the amplitude scattering matrices for two particles identical except for orientation.

It is convenient to introduce a coordinate system where the positive z direction coincides with $\hat{\mathbf{e}}_i$ (Fig. 13.11). Without loss of generality we may take the scattering plane to be the yz plane, in which instance the scattering amplitudes for two orthogonal polarization states of the incident light are (see Chapter 3, particularly Fig. 3.3 and Section 3.4)

$$\begin{aligned} \mathbf{A}(\hat{\mathbf{e}}_x; \hat{\mathbf{e}}_i, \hat{\mathbf{e}}_s) &= S_3 \hat{\mathbf{e}}_{\parallel s} + S_1 \hat{\mathbf{e}}_{\perp s}, \\ \mathbf{A}(\hat{\mathbf{e}}_y; \hat{\mathbf{e}}_i, \hat{\mathbf{e}}_s) &= S_2 \hat{\mathbf{e}}_{\parallel s} + S_4 \hat{\mathbf{e}}_{\perp s}. \end{aligned} \tag{13.10}$$

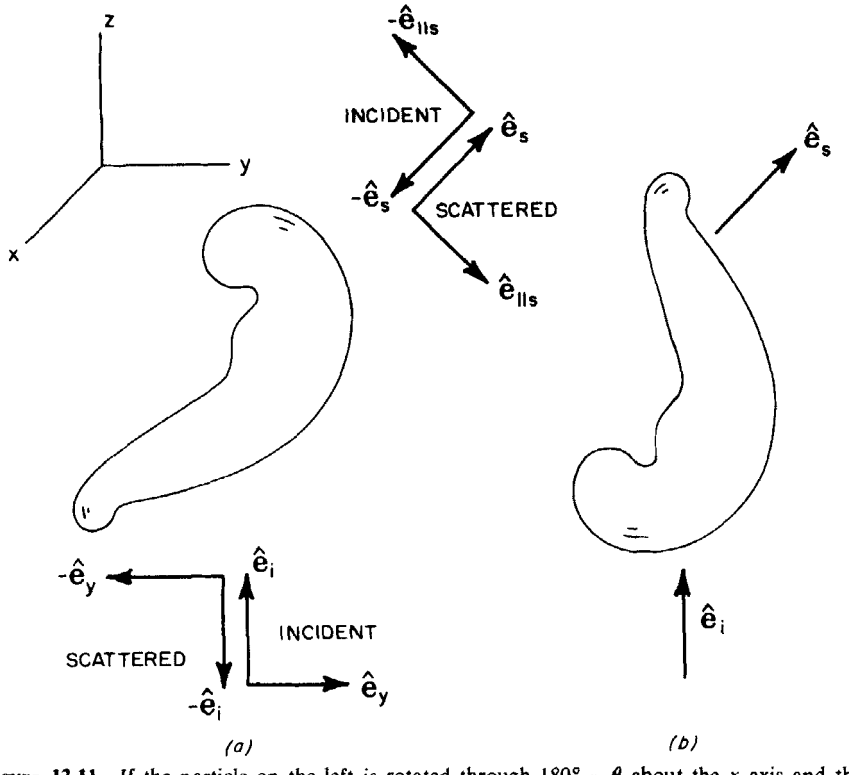

Figure 13.11 If the particle on the left is rotated through $180° - \theta$ about the x axis and then rotated through 180° about the z axis, the result is as shown on the right.

If the direction of the incident wave is now taken to be $-\hat{\mathbf{e}}_s$, the amplitudes of the waves scattered in the direction $-\hat{\mathbf{e}}_i$ for two orthogonal polarization states of the incident wave are

$$\mathbf{A}(-\hat{\mathbf{e}}_{\parallel s};\ -\hat{\mathbf{e}}_s, -\hat{\mathbf{e}}_i) = S_2'(-\hat{\mathbf{e}}_y) + S_4'\hat{\mathbf{e}}_x,$$

$$\mathbf{A}(\hat{\mathbf{e}}_{\perp s};\ -\hat{\mathbf{e}}_s, -\hat{\mathbf{e}}_i) = S_1'\hat{\mathbf{e}}_x + S_3'(-\hat{\mathbf{e}}_y). \tag{13.11}$$

It now follows trivially from (13.10), (13.11) and the reciprocity relation (13.9) that $S_1' = S_1$, $S_2' = S_2$, $S_3' = -S_4$, and $S_4' = -S_3$. The physical significance of the S_j' is that if the amplitude scattering matrix for an arbitrary particle is

$$\begin{pmatrix} S_2 & S_3 \\ S_4 & S_1 \end{pmatrix}, \tag{13.12}$$

then that for an identical particle rotated to bring $-\hat{\mathbf{e}}_s$ into congruence with $\hat{\mathbf{e}}_i$,

and $-\hat{\mathbf{e}}_i$ with $\hat{\mathbf{e}}_s$, is

$$\begin{pmatrix} S_2 & -S_4 \\ -S_3 & S_1 \end{pmatrix}. \tag{13.13}$$

The relative orientation of the two particles is shown in Fig. 13.11; note that the pairwise correspondence between the matrix (13.12) for the particle in position (a) and the matrix (13.13) for the same particle rotated into position (b) is specific to a given direction of observation $\hat{\mathbf{e}}_s$. If the direction of observation changes, then so, in general, does the orientation of the rotated particle; so the matrix (13.13) does not apply to a *single* rotated particle in a fixed orientation but rather to a *set* of identical particles in different orientations, one for every direction of observation.

To check (13.13) we can invoke the solution to the scattering problem for an optically active sphere. Such a sphere is symmetric under all rotations, but the off-diagonal elements of its scattering matrix (13.7) do not vanish identically. As required by symmetry and the matrices (13.12) and (13.13), (13.7) is invariant with respect to interchange and sign reversal of its off-diagonal elements.

We now direct our attention to the *mirror image* particle, obtained by reflection in the scattering plane, corresponding to an arbitrary particle. We showed in Section 8.3 that the circularly polarized components of the incident and scattered fields are related by

$$\begin{pmatrix} E_{Ls} \\ E_{Rs} \end{pmatrix} = \begin{pmatrix} S_{2c} & S_{3c} \\ S_{4c} & S_{1c} \end{pmatrix} \begin{pmatrix} E_{Li} \\ E_{Ri} \end{pmatrix}, \tag{13.14}$$

where we omit a multiplicative factor. The matrix elements in the circular polarization representation are connected to those in the linear polarization representation by a unitary transformation:

$$\begin{pmatrix} S_{1c} \\ S_{2c} \\ S_{3c} \\ S_{4c} \end{pmatrix} = \frac{1}{2} \begin{pmatrix} 1 & 1 & i & -i \\ 1 & 1 & -i & i \\ -1 & 1 & i & i \\ -1 & 1 & -i & -i \end{pmatrix} \begin{pmatrix} S_1 \\ S_2 \\ S_3 \\ S_4 \end{pmatrix}. \tag{13.15}$$

Reflection transforms right-circularly polarized light to left-circularly polarized light and conversely. Thus, under reflection $E_{Ls} \rightarrow E_{Rs}$, $E_{Rs} \rightarrow E_{Ls}$, and (13.14) becomes

$$\begin{pmatrix} E_{Rs} \\ E_{Ls} \end{pmatrix} = \begin{pmatrix} S'_{2c} & S'_{3c} \\ S'_{4c} & S'_{1c} \end{pmatrix} \begin{pmatrix} E_{Ri} \\ E_{Li} \end{pmatrix}. \tag{13.16}$$

It therefore follows that the matrix elements for the particle and its image are

related by

$$\begin{pmatrix} S_{1c} \\ S_{2c} \\ S_{3c} \\ S_{4c} \end{pmatrix} = \begin{pmatrix} 0 & 1 & 0 & 0 \\ 1 & 0 & 0 & 0 \\ 0 & 0 & 0 & 1 \\ 0 & 0 & 1 & 0 \end{pmatrix} \begin{pmatrix} S'_{1c} \\ S'_{2c} \\ S'_{3c} \\ S'_{4c} \end{pmatrix}. \tag{13.17}$$

It is now not difficult to show from (13.15) and (13.17) that if (13.12) is the scattering matrix for an arbitrary particle, then that for its mirror image is

$$\begin{pmatrix} S_2 & -S_3 \\ -S_4 & S_1 \end{pmatrix}. \tag{13.18}$$

Again, the exact solution to the optically active sphere problem provides us with an independent check of our analysis. Under reflection, the refractive indices m_L and m_R exchange roles and, as a consequence, the matrix element S_3 in (13.7) becomes $-S_3$; this is in accord with what is predicted by (13.18).

We shall need one more matrix, that for a particle obtained by the symmetry operations of reflection *and* rotation; this follows readily from (13.13) and (13.18):

$$\begin{pmatrix} S_2 & S_4 \\ S_3 & S_1 \end{pmatrix}. \tag{13.19}$$

The amplitude scattering matrices (13.12), (13.13), (13.18), and (13.19) for *single* particles related by the symmetry operations of reflection and rotation will find their greatest use in the following paragraphs on *collections* of particles.

13.6.2 Symmetries for Collections of Particles

The 4×4 scattering matrix for a collection of particles is the sum of all the scattering matrices for the individual particles in the collection provided that there is no systematic relation among the phases of the individual scattered waves (i.e., scattering is completely incoherent). In general, therefore, all 16 elements are independent. Symmetry, however, reduces the number of independent, nonzero matrix elements. In what follows we derive the form of the scattering matrix for collections of particles under very general assumptions, proceeding from less to more symmetry.

Although the term "collection" usually implies a system of many particles, our symmetry considerations apply equally well to a single particle randomized by tumbling or some other means. That is, our averages can equally well be taken as either time averages or ensemble averages. Suppose that in a collection of identical particles all orientations are equally probable. This implies that, for every scattering direction, if there is a particle with amplitude scattering matrix (13.12), it is certain that another particle is oriented so that its scattering matrix has the form (13.13). Thus, to determine 4×4 scattering

matrix symmetries, we need consider only pairs of particles. One example will suffice. It follows from (3.16), (13.12), and (13.13) that both the S_{12} and S_{21} matrix elements for a pair of particles are equal to $|S_2|^2 - |S_1|^2$. In a like manner we can find all the other symmetry relations. The result is a 10-parameter scattering matrix:

$$\begin{pmatrix} S_{11} & S_{12} & S_{13} & S_{14} \\ S_{12} & S_{22} & S_{23} & S_{24} \\ -S_{13} & -S_{23} & S_{33} & S_{34} \\ S_{14} & S_{24} & -S_{34} & S_{44} \end{pmatrix}. \tag{13.20}$$

This is the form of the scattering matrix for any medium with rotational symmetry even if all the particles are not identical in shape and composition. A collection of optically active spheres is perhaps the simplest example of a particulate medium which is symmetric under all rotations but not under reflection. Mirror asymmetry in a collection of randomly oriented particles can arise either from the shape of the particles (corkscrews, for example) or from optical activity (circular birefringence and circular dichroism).

Let us now increase the degree of symmetry. As in the previous paragraph, the particles are identical and randomly oriented, but with the additional property that each particle can be brought into congruence with its reflection in any scattering plane by a suitable rotation. This excludes particles with intrinsic optical activity, although linear birefringence and dichroism are permissible. With these assumptions, the collection can be grouped into quartets each particle of which is associated with one of the amplitude scattering matrices (13.12), (13.13), (13.18), or (13.19). Thus, the sum of the scattering matrices for these four particles gives us the form of the scattering matrix for the collection. Again, one example should be sufficient: both S_{34} and $-S_{43}$ for a quartet are equal to $2\,\mathrm{Im}\{S_2 S_1^*\}$. All the other matrix symmetries follow from a similar set of calculations obtained with (3.16) and the four amplitude scattering matrices. The final result is a matrix with eight nonzero elements, six of which are independent:

$$\begin{pmatrix} S_{11} & S_{12} & 0 & 0 \\ S_{12} & S_{22} & 0 & 0 \\ 0 & 0 & S_{33} & S_{34} \\ 0 & 0 & -S_{34} & S_{44} \end{pmatrix}. \tag{13.21}$$

Scattering media to which this matrix applies include randomly oriented anisotropic spheres of substances such as calcite or crystalline quartz (uniaxial) or olivine (biaxial). Also included are isotropic cylinders and ellipsoids of substances such as glass and cubic crystals. An example of an exactly soluble system to which (13.21) applies is scattering by randomly oriented isotropic spheroids (Asano and Sato, 1980). Elements of (13.21) off the block diagonal vanish. Some degree of alignment is implied, therefore, if these matrix elements

do not vanish for a collection of isotropic elongated particles with mirror symmetry.

The matrix (13.21) is not restricted, however, to collections of particles each of which is congruent with its mirror image; it applies equally well to any medium that is invariant under rotation and reflection, which includes the possibility of mirror asymmetric particles each of which is paired with its image in the appropriate orientation.

Scattering matrices for collections of isotropic spherical particles have the greatest degree of symmetry. Regardless of size and composition, the scattering matrix for such particles—this includes inhomogeneous particles—has the form (13.6). There are eight nonzero elements; four of them, at most, are independent. Examples are spherical liquid droplets and solid spheres composed either of amorphous solids such as glass and silica or crystalline solids with cubic symmetry such as MgO and NaCl. Note that S_{11} and S_{22} are equal (as are S_{33} and S_{44}) in (13.6). If, therefore, cross polarization is detected in a measurement of angular scattering, this is sufficient to rule out isotropic spheres.

It is sometimes asserted that randomly oriented nonspherical particles are somehow equivalent to spherical particles—it is just a matter of choosing the correct size distribution. This reasoning is based, perhaps, on the realization that both systems are spherically symmetrical. But an inescapable conclusion to be drawn from the preceding paragraphs is that this assertion cannot be strictly true: regardless of the size and composition of the "equivalent" spheres, symmetry precludes full equivalence.

13.7 MEASUREMENT TECHNIQUES FOR THE SCATTERING MATRIX

The simplest, and probably most obvious, way to measure scattering matrix elements is with a conventional nephelometer (Fig. 13.5) and various optical elements fore and aft of the scattering medium. Recall that we introduced Stokes parameters in Section 2.11 by way of a series of conceptual measurements of differences between irradiances with different polarizers in the beam. Although we did not specify the origin of the beam, it could be light scattered in any direction. Combinations of scattering matrix elements can therefore be extracted from these kinds of measurements. There are now, however, two beams—incident and scattered—and many possible pairs of optical elements; these are discussed below.

We list in Table 13.1 all the possible measured irradiances (for unit incident irradiance) with a polarizer before the scattering medium and an analyzer before the detector. The light transmitted by an ideal polarizer P_s is polarized in state s: R and L denote right-circular and left-circular polarization; $\parallel$ and $\perp$ denote light polarized parallel and perpendicular to the scattering plane; $+$ and $-$ denote light polarized obliquely to the scattering plane at $+45°$ and $-45°$. U denotes the absence of a polarizer or analyzer; if U is indicated as

Table 13.1 Combinations of Scattering Matrix Elements That Result from Measurements with a Polarizer P_s Forward of the Scattering Medium and an Analyzer A_s aft[a]

U	U	S_{11}	$P_\perp$	U	$\frac{1}{2}(S_{11} - S_{12})$
U	$A_\parallel$	$\frac{1}{2}(S_{11} + S_{21})$	$P_\perp$	$A_\parallel$	$\frac{1}{4}(S_{11} - S_{12} + S_{21} - S_{22})$
U	$A_\perp$	$\frac{1}{2}(S_{11} - S_{21})$	$P_\perp$	$A_\perp$	$\frac{1}{4}(S_{11} - S_{12} - S_{21} + S_{22})$
U	A_+	$\frac{1}{2}(S_{11} + S_{31})$	$P_\perp$	A_+	$\frac{1}{4}(S_{11} - S_{12} + S_{31} - S_{32})$
U	A_-	$\frac{1}{2}(S_{11} - S_{31})$	$P_\perp$	A_-	$\frac{1}{4}(S_{11} - S_{12} - S_{31} + S_{32})$
U	A_R	$\frac{1}{2}(S_{11} - S_{41})$	$P_\perp$	A_R	$\frac{1}{4}(S_{11} - S_{12} - S_{41} + S_{42})$
U	A_L	$\frac{1}{2}(S_{11} + S_{41})$	$P_\perp$	A_L	$\frac{1}{4}(S_{11} - S_{12} + S_{41} - S_{42})$
$P_\parallel$	U	$\frac{1}{2}(S_{11} + S_{12})$	P_+	U	$\frac{1}{2}(S_{11} + S_{13})$
$P_\parallel$	$A_\parallel$	$\frac{1}{4}(S_{11} + S_{12} + S_{21} + S_{22})$	P_+	$A_\parallel$	$\frac{1}{4}(S_{11} + S_{13} + S_{21} + S_{23})$
$P_\parallel$	$A_\perp$	$\frac{1}{4}(S_{11} + S_{12} - S_{21} - S_{22})$	P_+	$A_\perp$	$\frac{1}{4}(S_{11} + S_{13} - S_{21} - S_{23})$
$P_\parallel$	A_+	$\frac{1}{4}(S_{11} + S_{12} + S_{31} + S_{32})$	P_+	A_+	$\frac{1}{4}(S_{11} + S_{13} + S_{31} + S_{33})$
$P_\parallel$	A_-	$\frac{1}{4}(S_{11} + S_{12} - S_{31} - S_{32})$	P_+	A_-	$\frac{1}{4}(S_{11} + S_{13} - S_{31} - S_{33})$
$P_\parallel$	A_R	$\frac{1}{4}(S_{11} + S_{12} - S_{41} - S_{42})$	P_+	A_R	$\frac{1}{4}(S_{11} + S_{13} - S_{41} - S_{43})$
$P_\parallel$	A_L	$\frac{1}{4}(S_{11} + S_{12} + S_{41} + S_{42})$	P_+	A_L	$\frac{1}{4}(S_{11} + S_{13} + S_{41} + S_{43})$
P_-	U	$\frac{1}{2}(S_{11} - S_{13})$	P_L	U	$\frac{1}{2}(S_{11} - S_{14})$
P_-	$A_\parallel$	$\frac{1}{4}(S_{11} - S_{13} + S_{21} - S_{23})$	P_L	$A_\parallel$	$\frac{1}{4}(S_{11} - S_{14} + S_{21} - S_{24})$
P_-	$A_\perp$	$\frac{1}{4}(S_{11} - S_{13} - S_{21} + S_{23})$	P_L	$A_\perp$	$\frac{1}{4}(S_{11} - S_{14} - S_{21} + S_{24})$
P_-	A_+	$\frac{1}{4}(S_{11} - S_{13} + S_{31} - S_{33})$	P_L	A_+	$\frac{1}{4}(S_{11} - S_{14} + S_{31} - S_{34})$
P_-	A_-	$\frac{1}{4}(S_{11} - S_{13} - S_{31} + S_{33})$	P_L	A_-	$\frac{1}{4}(S_{11} - S_{14} - S_{31} + S_{34})$
P_-	A_R	$\frac{1}{4}(S_{11} - S_{13} - S_{41} + S_{43})$	P_L	A_R	$\frac{1}{4}(S_{11} - S_{14} - S_{41} + S_{44})$
P_-	A_L	$\frac{1}{4}(S_{11} - S_{13} + S_{41} - S_{43})$	P_L	A_L	$\frac{1}{4}(S_{11} - S_{14} + S_{41} - S_{44})$
P_R	U	$\frac{1}{2}(S_{11} + S_{14})$			
P_R	$A_\parallel$	$\frac{1}{4}(S_{11} + S_{14} + S_{21} + S_{24})$			
P_R	$A_\perp$	$\frac{1}{4}(S_{11} + S_{14} - S_{21} - S_{24})$			
P_R	A_+	$\frac{1}{4}(S_{11} + S_{14} + S_{31} + S_{34})$			
P_R	A_-	$\frac{1}{4}(S_{11} + S_{14} - S_{31} - S_{34})$			
P_R	A_R	$\frac{1}{4}(S_{11} + S_{14} - S_{41} - S_{44})$			
P_R	A_L	$\frac{1}{4}(S_{11} + S_{14} + S_{41} + S_{44})$			

[a] U indicates the absence of a polarizer or analyzer.

being before the scattering medium, we assume that the incident light is completely unpolarized, which is an idealization. The linear analyzers $A_\parallel, \ldots, A_-$ are identical with the linear polarizers $P_\parallel, \ldots, P_-$. The circular analyzers A_R and A_L, however, are the circular polarizers P_R and P_L taken in reverse order. A circular polarizer or analyzer is a composite of two optical elements—a linear polarizer and a $\pm 90°$ retarder—the order of which in the optical train is important: if the beam first encounters the linear polarizer, then the composite is a circular polarizer; the reverse order gives a circular analyzer. We have not made a distinction between polarizers and analyzers in previous sections of this book. In this instance, however, such a distinction seems desirable to avoid

confusion. Mueller matrices for polarizers and retarders are given in Section 2.11.

The possible outcomes of measurements—combinations of scattering matrix elements—listed in Table 13.1 follow from multiplication of three matrices: those representing the polarizer, the scattering medium, and the analyzer. If U is an element in the optical train, then the measured irradiance depends on only two matrix elements. In general, however, there are four elements in a combination, so that four measurements are required to obtain one matrix element.

Scattering matrix elements were measured in this manner by Pritchard and Elliot (1960) and by Holland and Gagne (1970); the former authors gave results similar to those in Table 13.1 for a medium with scattering matrix (13.21). Although this technique is straightforward, albeit possibly laborious, relative errors can be appreciable when two large signals are subtracted to obtain small matrix elements—S_{13} and S_{14}, for example. Subtraction can be avoided by amplifying the detector signal modulated by rotating a polarizer or retarder in either the incident or scattered beam. Sekera (1957) described such a method for measuring skylight polarization. It can be an improvement over subtractive techniques. But it has disadvantages: the element cannot always be rotated as fast as desired; imperfections, such as scratches or dust on the rotating element, spuriously modulate the signal, which limits sensitivity. There is, however, a polarization modulation technique, without rotating elements, for measuring angular scattering; this is described in the following paragraphs.

The heart of the polarization-modulated nephelometer is a photoelastic modulator, developed by Kemp (1969) and by Jasperson and Schnatterly (1969). The latter used their instrument for ellipsometry of light reflected by solid surfaces (the application described here could be considered as ellipsometry of scattered light). Kemp first used the modulation technique in laboratory studies but soon found a fertile field of application in astrophysics: the modulator, coupled with a telescope, allowed circular polarization from astronomical objects to be detected at much lower levels than previously possible.

The photoelastic modulator is composed of a piezoelectric transducer coupled to a block of amorphous quartz. The transducer, a quartz crystal, is driven by an electric field oscillating at a characteristic frequency set by the crystal dimensions (typically 50 kHz). Periodic stress birefringence is therefore induced in the amorphous quartz block. If light incident on the modulator is linearly polarized at 45° to its axis, the polarization state of the transmitted light alternates between left circular and right circular provided that the amplitude of the induced stress is sufficient to give 90° retardance. This rapid polarization-modulation technique permits phase-sensitive detection of discrete Fourier components of the scattered light and avoids problems commonly encountered with rotating elements.

A photoelastic modulator mated to a nephelometer is shown schematically in Fig. 13.12 (Hunt and Huffman, 1973, 1975; Perry et al., 1978). The transmission axis of the linear polarizer P is fixed at 45° relative to the stress

axis of the modulator M, which may be at either 0° or 45° to the scattering plane. Light transmitted by the modulator is scattered by the sample S and then detected after (possibly) passing through the analyzer A mounted on the scanning arm. We shall illustrate the operation of this system in the configuration for determining the matrix elements S_{12} and S_{14}: the modulator is at 45° to the scattering plane and there is no analyzer. The sequence of matrix multiplications representing the transformations of the light as it traverses the system is given below.

Scattering Sample *Retarder* *Polarizer*

$$\begin{pmatrix} S_{11} & S_{12} & S_{13} & S_{14} \\ S_{21} & S_{22} & S_{23} & S_{24} \\ S_{31} & S_{32} & S_{33} & S_{34} \\ S_{41} & S_{42} & S_{43} & S_{44} \end{pmatrix} \begin{pmatrix} 1 & 0 & 0 & 0 \\ 0 & \cos\delta & 0 & -\sin\delta \\ 0 & 0 & 1 & 0 \\ 0 & \sin\delta & 0 & \cos\delta \end{pmatrix} \frac{1}{2}\begin{pmatrix} 1 & 1 & 0 & 0 \\ 1 & 1 & 0 & 0 \\ 0 & 0 & 0 & 0 \\ 0 & 0 & 0 & 0 \end{pmatrix}$$

The incident beam, which we may take to be unpolarized, encounters three optical elements, each of which is represented by a matrix; we recall from Section 2.11 that matrices for polarizers and retarders depend on their orientation. The Stokes parameters of the light emerging successively from the polarizer, the modulator, and the scattering sample are (from right to left)

After S *After M* *After P*

$$\frac{1}{2}\begin{pmatrix} S_{11}+S_{12} & \cos\delta + S_{14} & \sin\delta \\ S_{21}+S_{22} & \cos\delta + S_{24} & \sin\delta \\ S_{31}+S_{32} & \cos\delta + S_{34} & \sin\delta \\ S_{41}+S_{42} & \cos\delta + S_{44} & \sin\delta \end{pmatrix} \frac{1}{2}\begin{pmatrix} 1 \\ \cos\delta \\ 0 \\ \sin\delta \end{pmatrix} \frac{1}{2}\begin{pmatrix} 1 \\ 1 \\ 0 \\ 0 \end{pmatrix}$$

The detector response is proportional to the first Stokes parameter

$$\tfrac{1}{2}C(S_{11} + S_{12}\cos\delta + S_{14}\sin\delta),$$

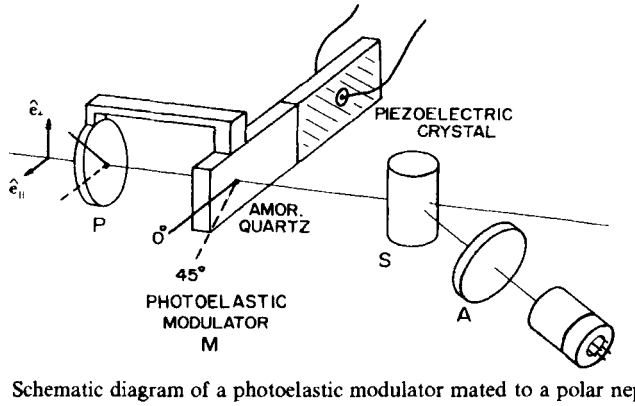

Figure 13.12 Schematic diagram of a photoelastic modulator mated to a polar nephelometer.

where C is a constant that incorporates such factors as light-collecting efficiency and detector sensitivity. The signal is time dependent because of the variable retardance

$$\delta = \frac{2\pi d}{\lambda} s \sin \omega t = A \sin \omega t,$$

where d is the thickness of the modulator, λ is the wavelength, ω is the frequency of the electric field driving the modulator, and s is proportional to the stress-optical constant and the amplitude of the induced stress (Born and Wolf, 1965, p. 705). The trigonometric functions of retardance can be expanded in series of Bessel functions

$$\sin(A \sin \omega t) = 2J_1(A)\sin \omega t + 2J_3(A)\sin 3\omega t + \cdots$$

$$\cos(A \sin \omega t) = J_0(A) + 2J_2(A)\cos 2\omega t + \cdots$$

If the modulator amplitude is adjusted so that $J_0(A) = 0$, the detector signal is

$$\tfrac{1}{2}C\{S_{11} + 2S_{12}J_2(A)\cos 2\omega t + 2S_{14}J_1(A)\sin \omega t + \cdots\}$$

$$= \frac{1}{2}CS_{11}\left\{1 + \frac{S_{12}}{S_{11}}2J_2(A)\cos 2\omega t + \frac{S_{14}}{S_{11}}2J_1(A)\sin \omega t + \cdots\right\}.$$

Factoring out of S_{11} is accomplished in practice by electronically servoing the dc signal to a constant value which, in effect, normalizes the terms by S_{11}. The signal therefore has components proportional to S_{14}/S_{11} and S_{12}/S_{11}, which oscillate at frequencies ω and 2ω, respectively. These two components are separated by phase-sensitive detection, that is, by "locking in" on either ω or 2ω. The instrument is calibrated by replacing the sample with a linear polarizer or a quarter-wave plate and adjusting the servo gain for 100% signal in the forward direction.

A great advantage of this type of system is that it makes possible measurements of relatively small matrix elements such as S_{14}: the signal can be amplified as necessary because only one component is proportional to S_{14}. Normalization by S_{11}, which is done electronically, eliminates fluctuations in particle number density and in the light source. If S_{11} is desired, the electronic servo can be turned off and the instrument used in the conventional way.

An alternative configuration is the polarizer–modulator placed before the detector rather than the sample. This might be useful for measurements in the atmosphere; for example, a searchlight as the light source with the modulator at or near the focus of a portable telescope followed by a detector. For laboratory investigations it is also sometimes convenient to place the modulator before the detector.

A disadvantage of the system described in the preceding paragraphs is that, in general, the time-harmonic components of the signal contain mixtures of

matrix elements. With the modulator either forward or aft of the sample, only matrix elements in the first row and column can be measured individually; mixing occurs for the other nine elements. For example, an attempt to measure S_{34}/S_{11} yields $(S_{34} + S_{14})/(S_{11} + S_{31})$. This is not always a problem because S_{14} and S_{31} are zero for many collections of particles (see Section 13.6). If S_{14} and S_{31} are not zero they can, of course, be measured individually and used to extract S_{34}/S_{11} from measurements; but to a certain extent this nullifies the advantages of the modulation system.

Mixing of matrix elements can be avoided with more complicated systems having one or more modulators, driven at different frequencies, in both the entrance and exit beams. Azzam (1978) considered the general planning of such nephelometers for measuring all 16 elements simultaneously, which is possible only if both the entrance and exit beams are modulated. Thompson et al. (1980) constructed a system for measuring all 16 elements simultaneously. Four Pockels-cell modulators of different frequencies are used, two each in the entrance and exit beams. The resulting signal is a sum of time-harmonic terms where the amplitude of each term is proportional to a single matrix element.

13.8 SOME RESULTS FOR THE SCATTERING MATRIX

Few measurements or calculations of all 16 scattering matrix elements have been reported. There are only four nonzero independent elements for spherical particles and six for a collection of randomly oriented particles with mirror symmetry (Section 13.6). It is sometimes worth the effort, however, to determine if the expected equalities and zeros really occur. If they do not, this may signal interesting properties such as deviations from sphericity, unexpected asymmetry, or partial alignment; some examples are given in this section. But we begin with spherical particles.

13.8.1 Polystyrene Spheres and Water Droplets

Measurements of four matrix elements made with the polarization modulation instrument described in the preceding section are shown in Fig. 13.13. The curves on the left are for an aqueous suspension of polystyrene spheres narrowly distributed in size; on the right are the same matrix elements for a broad size distribution of water droplets made with an ultrasonic nebulizer (Hunt and Huffman, 1975). Many peaks and valleys appear in all the matrix elements for the polystyrene spheres; the curves in Figs. 13.1 and 13.2 demonstrated that such structure is very sensitive to size and refractive index and thus can be used to determine these quantities either for single spheres or narrow size distributions. Structure is largely absent from the water droplet curves, however, and only general features remain. Around 150°, for example, there is broad structure in all four matrix elements; this is the onset of the fog bow, or cloud bow, a feature that develops into the rainbow for larger droplets (Fig. 13.4). Note that the S_{11} signal is noisy because the number of particles in

the scattering volume fluctuates; this noise is removed electronically from the other matrix elements by normalization. Because of normalization the number of droplets in the beam is not important provided that multiple scattering is negligible.

Quiney and Carswell (1972) made measurements on artificial fogs and reported that S_{33}/S_{11} and S_{34}/S_{11} showed more pronounced differences from one fog to another than did the more commonly measured matrix elements such as S_{12}/S_{11}. Hunt and Huffman (1975) suggested the possibility of using S_{34}/S_{11} at a single angle near 95° to monitor the mean size of nebulized water droplets. Because little use has been made of all matrix elements, however, a systematic study of their relative merits in determining size distributions has not been made.

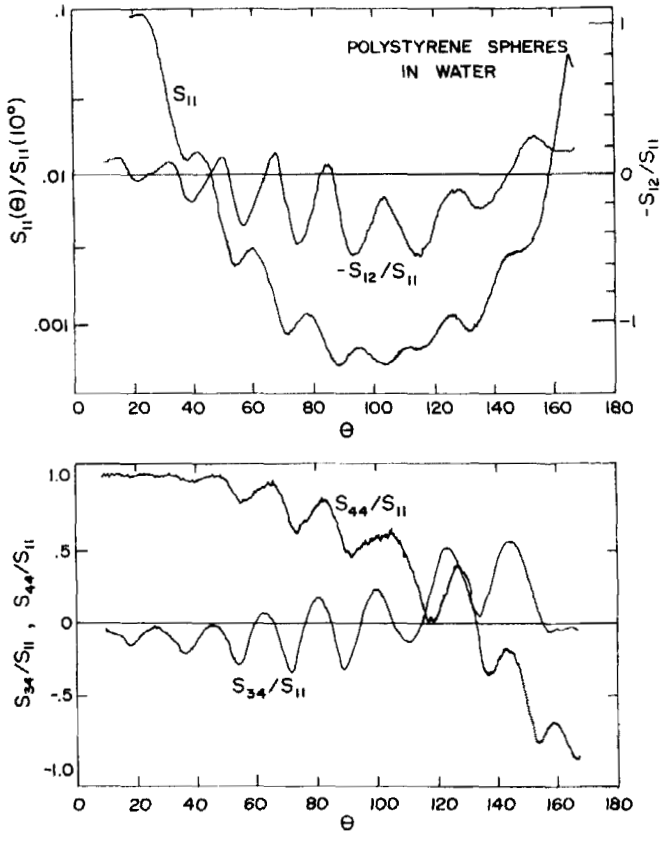

Figure 13.13 Measured matrix elements (left) for polystyrene spheres in water (mean radius 0.40 μm, wavelength 0.3250 μm). Measured matrix elements (right) for water droplets (mean radius 1.5 μm, wavelength 0.6328 μm). From Hunt and Huffman (1975).

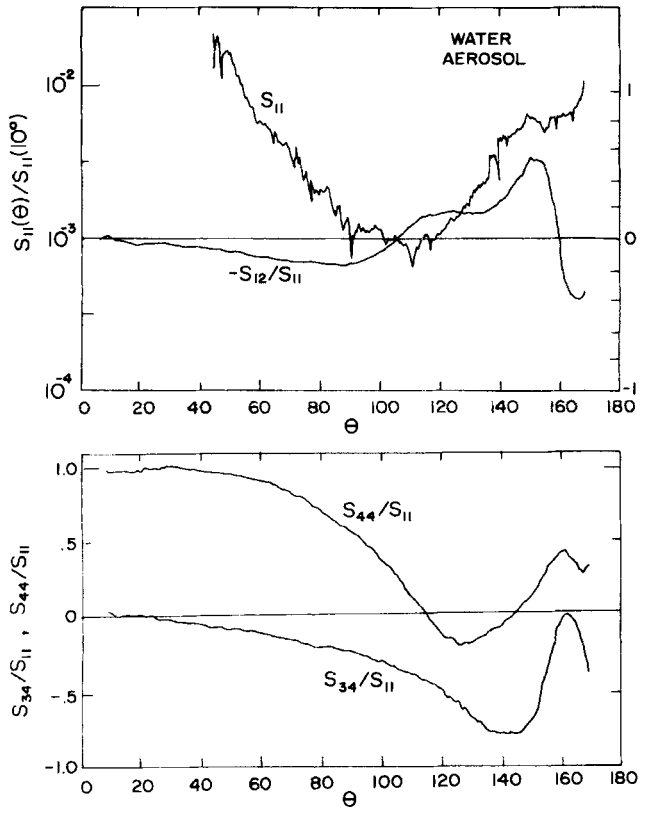

Figure 13.13 (*Continued*)

Sekera (1957) and Rozenberg (1960) emphasized the importance of measuring all matrix elements for atmospheric aerosols, and a few such measurements have been reported (Pritchard and Elliot, 1960; Beardsley, 1968; Golovanev et al., 1971). With sensitive modulation techniques it should indeed be possible to probe atmospheric particles remotely using the complete scattering matrix to infer not only size distributions but also refractive indices. Care must be exercised, however, because nonsphericity can lead to false inferences about absorption: analysis based on Mie theory cannot disentangle the two effects.

13.8.2 Nonspherical Particles

One of the few sets of measurements of all scattering matrix elements for nonspherical particles was made by Holland and Gagne (1970), who used various combinations of polarizers and retarders (see Section 13.7). They studied quartz (sand) particles with a fairly broad range of sizes. To investigate further the effects of nonsphericity on all matrix elements Perry et al. (1978),

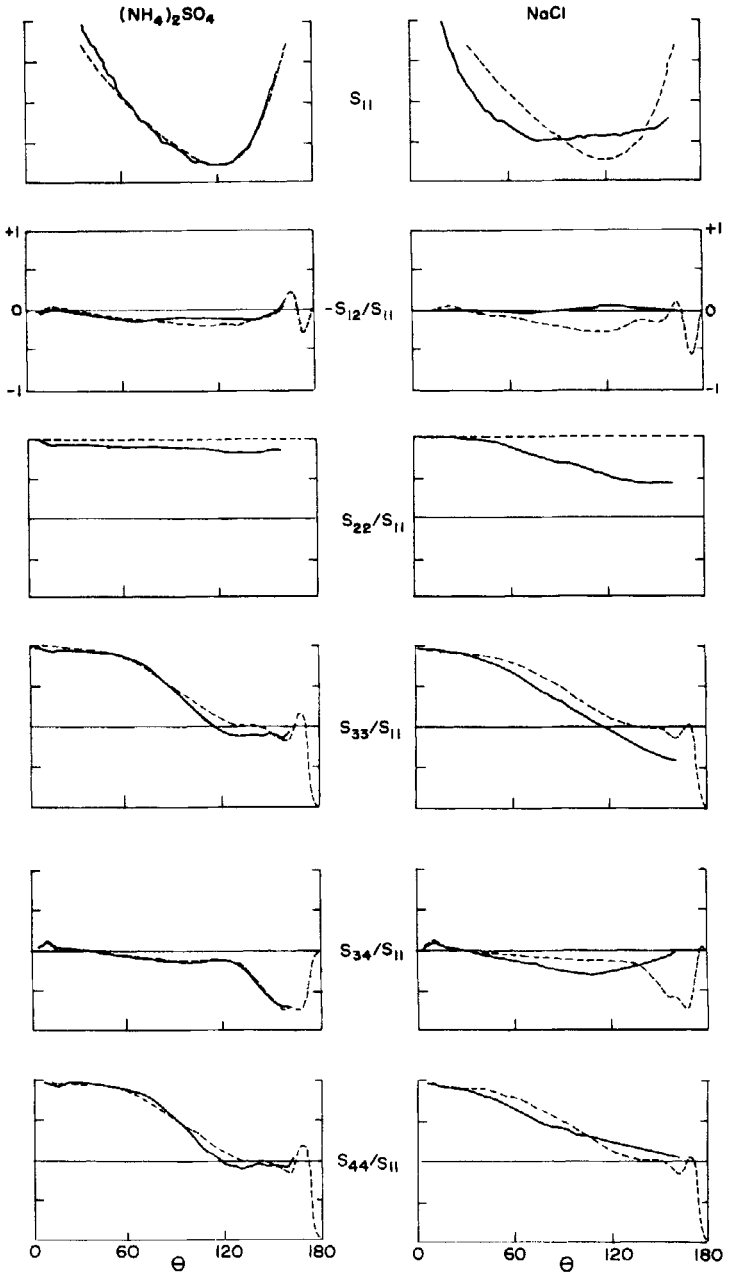

Figure 13.14 The six independent matrix elements for two aerosols. Solid lines are measurements from Perry et al. (1978); dashed lines are theoretical (we redid their calculations).

using the polarization modulation technique, studied two aerosols, both with a mean radius of about 0.63 μm and a fractional standard deviation of about 0.3, but differing in shape: rounded (but not perfectly spherical) ammonium sulfate particles and nearly cubic sodium chloride particles; they were made by nebulizing solutions of these salts and drying the droplets in a nitrogen stream. Eight matrix elements were determined to be zero within experimental accuracy, as expected; the remaining elements, for incident light of wavelength 0.3250 μm, are shown in Fig. 13.14. Because the size distributions and refractive indices of the two aerosols are similar, comparison of their matrix elements clearly shows the effect of shape.

Although S_{11} calculated from Mie theory has been adjusted arbitrarily relative to the measurements, it is obvious that cubic particles are poorly described by theory for spheres; this is in contrast with the data for the rounded particles, which agree well with calculations. S_{11} for the cubes is nearly constant at scattering angles greater than about 90° and does not rise sharply in the backscattering direction as it does for the rounded particles; this was pointed out in connection with Fig. 13.8. Positive polarization ($-S_{12}/S_{11}$) and appreciable deviations of S_{22}/S_{11} from unity for cubes were also discussed in Section 13.4. Note the small deviations of S_{22}/S_{11} from unity for the rounded particles. S_{22}/S_{11}, which is essentially the cross polarization, is one for spheres at all scattering angles; therefore, a single measurement of this quantity at some large angle could provide a simple and sensitive test of nonsphericity.

In the three matrix elements shown in the bottom half of Fig. 13.14, there appear to be less pronounced differences between spheres and nonspherical particles. Perry et al. pointed out that near the forward direction S_{34}/S_{11} is rather sensitive to the parameters of the size distribution, while measurements for both kinds of particles—rounded and cubic—agree quite well with calculations. Similar agreement between calculations for spheres and spheroids was noted by Asano and Sato (1980). This combination of sensitivity to size distribution and insensitivity to shape might be put to good use in particle sizing.

13.8.3 Clusters of Spheres

Shape effects caused by aggregation played an important part in our discussion of surface modes in Chapter 12. When two or more identical spheres aggregate into a cluster the resulting composite particle is nonspherical. As a consequence it must be expected to scatter light differently from its constituent spheres. In an experimental effort that reveals much about light scattering by nonspherical particles, Bottiger et al. (1980) measured all scattering matrix elements for single polystyrene spheres and clusters of two, three, and four similar spheres. A sphere or cluster of spheres was suspended in an electrostatic levitation chamber and all matrix elements were measured simultaneously using the instrument mentioned at the end of Section 13.7. Measured

zeros for the eight elements off the block diagonal ($S_{13}, \ldots, S_{42}$) confirmed that the particles assumed all orientations during a measurement.

A series of measurements for single spheres and clusters is shown in Fig. 13.15. Large oscillations in S_{12}/S_{11} for a single sphere diminish in amplitude as the cluster size increases, although remnants of the single-particle signal are still evident. Other normalized matrix elements (S_{33}, S_{44}, S_{43}) show a similar trend toward subdued structure as the cluster size increases. The normalized S_{22} matrix element for the clusters decreases with increasing scattering angle, and the rate of decrease increases with increasing cluster size; this further confirms that deviation of S_{22}/S_{11} from unity is a clear indication of nonspher-

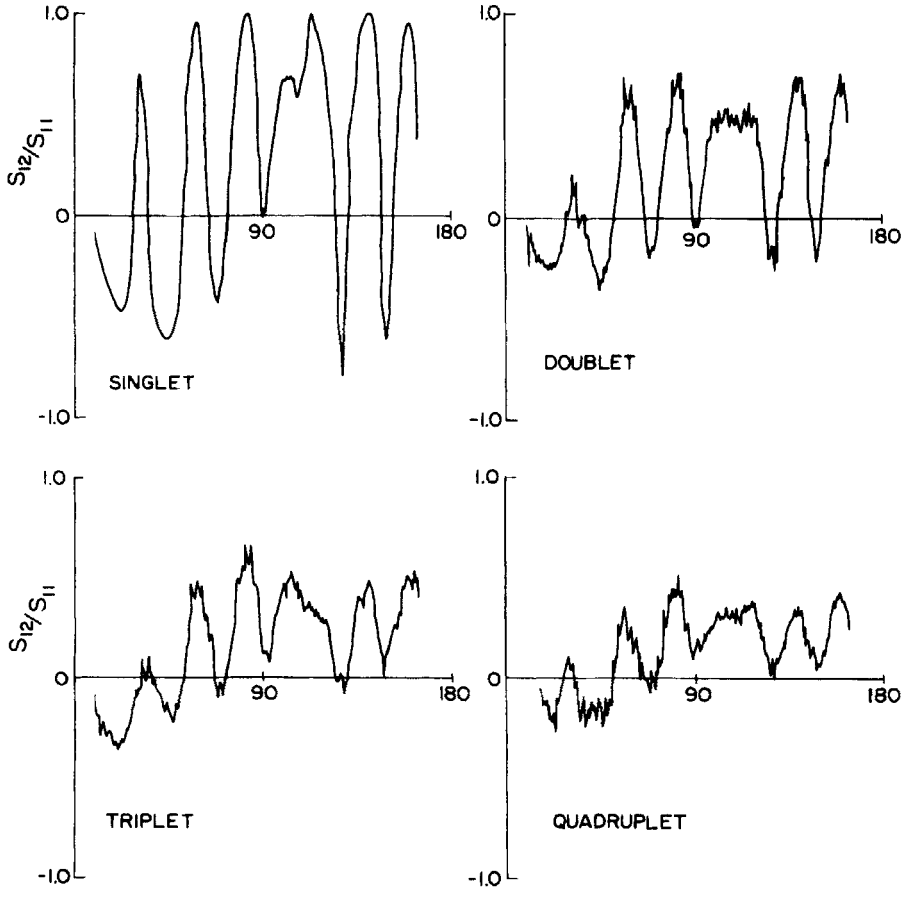

Figure 13.15 Angular dependence of S_{12}/S_{11} measured for a single polystyrene sphere of radius 1091 nm and for clusters of two, three, and four similar spheres; the wavelength of the incident light is 441.6 nm. From Bottiger et al. (1980).

icity. S_{33} and S_{44} are identical for spheres but show noticeable differences for the larger clusters.

13.8.4 Quartz Fibers

Bell (1981) (see also Bell and Bickel, 1981) measured all matrix elements for fused quartz fibers of a few micrometers in diameter with a photoelastic polarization modulator similar to that of Hunt and Huffman (1973); the HeCd (441.6 nm) laser beam was normal to the fiber axes. Advantages of fibers as single-particle scattering samples are their orientation is readily fixed and they can easily be manipulated and stored. Two of the four elements for a 0.96-μm-radius fiber are shown in Fig. 13.16; dots represent measurements and solid lines were calculated using an earlier version of the computer program in Appendix C. Bell was able to determine the fiber radius to within a few tenths of a percent by varying the radius in calculations, assuming a refractive index of $1.446 + i0.0$, until an overall best fit to the measured matrix elements was obtained.

13.8.5 Biological Particles

Angular light scattering is a widely used nondestructive technique for studying particles of biological origin such as viruses, bacteria, and eucaryotic cells. Measurements of all scattering matrix elements for such particles, however, are rare. An exception is the work of Bickel et al. (1976) and Bickel and Stafford (1980), who measured all matrix elements for a variety of biological particles. A striking result of this work is that S_{34}/S_{11} proved to be uniquely characteristic of each biological scatterer. Reproducible differences in S_{34}/S_{11} were found for particles that could not readily be distinguished by other common techniques.

Differences in the S_{34}/S_{11} signals for two mutant varieties of bacterial spores differing in a specific structural mutation are obvious in Fig. 13.17. Other matrix elements, however, are less obviously different for the two similar scatterers. To first approximation scattering by biological particles tends to be described well by Rayleigh–Gans theory (Chapter 6) for which $S_{34} = 0$. Within the framework of this theory elements off the block diagonal are also zero, as they are for larger and more refractive arbitrary particles provided that their scattering matrix has the symmetry (13.21). Thus, S_{34} is the matrix element that is likely to undergo the greatest relative change as a particle's characteristics deviate more and more from those for which the Rayleigh–Gans theory is valid. This may be the reason S_{34}/S_{11} is so sensitive to characteristics of biological scatterers.

13.8.6 Ocean Waters

All 16 matrix elements for natural ocean waters have been measured using combinations of polarizing and retarding elements (Kadyshevich et al., 1971,

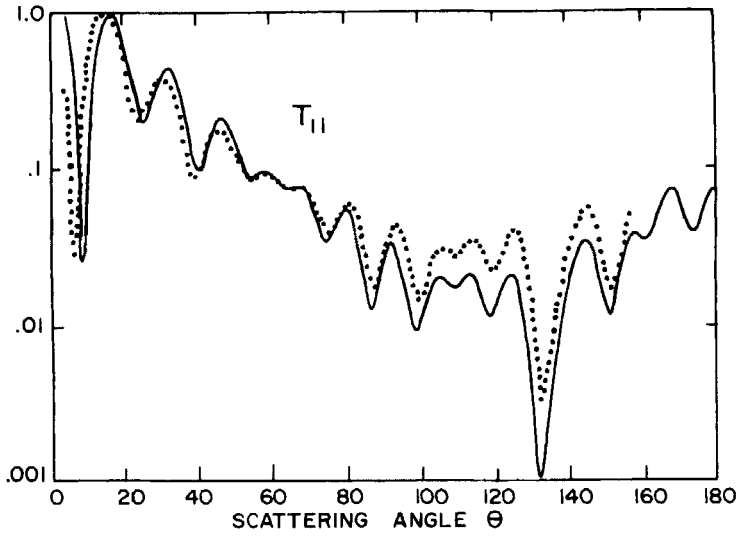

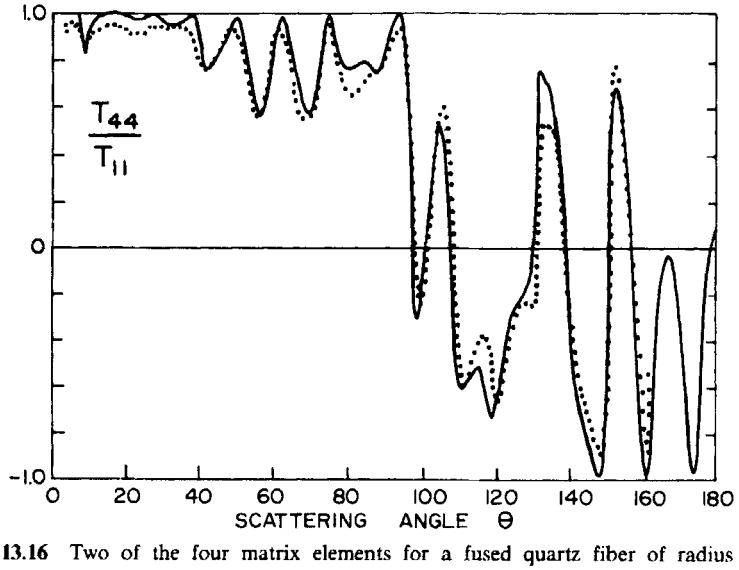

Figure 13.16 Two of the four matrix elements for a fused quartz fiber of radius 0.96 μm illuminated by light of wavelength 0.4416 μm. The solid curves are calculations, the dots are measurements. From Bell (1981).

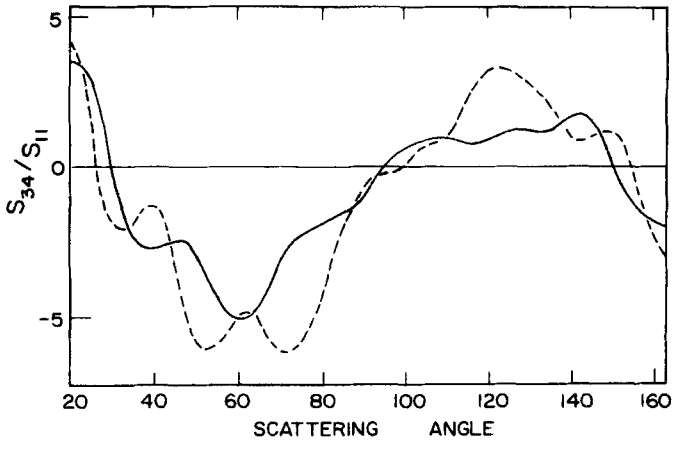

Figure 13.17 Angular dependence of S_{34}/S_{11} (percent) for two similar bacterial spores. From Bickel et al. (1976).

1976). A surprising result of this work is that the scattering matrix, particularly for Pacific Ocean waters, has none of the symmetries discussed in Section 13.6. Only the normalized elements S_{13}/S_{11} and S_{43}/S_{11} were determined to be zero within experimental accuracy; all others had appreciable values. Further, there were substantial differences among matrix elements and in matrix symmetry for different ocean waters (Atlantic and Pacific) and for Baltic Sea waters. The unusual symmetry of the scattering matrix seems to demand partial alignment of asymmetric particles by, for example, gravitational or magnetic fields.

Measurements by Thompson et al. (1978) on cultured populations of phytoplankton, such as might be expected to scatter light in ocean waters, revealed only a scattering matrix of the form (13.5), characteristic of particles for which either the Rayleigh (Chapter 5) or Rayleigh–Gans (Chapter 6) approximations are valid.

So we end this section with unanswered questions: Do the unusual scattering matrices measured by the Russian investigators really exist in nature, or are they merely experimental artifacts? If the former, how is this reconciled with the measurements of Thompson et al.?

13.9 SUMMARY: APPLICABILITY OF MIE THEORY

At the present time the electromagnetic scattering theory for a sphere, which we have called Mie theory, provides the only practical method for calculating light-scattering properties of finite particles of arbitrary size and refractive index. Clearly, however, many particles of interest are not spheres. It is therefore of considerable importance to know the extent to which Mie theory is applicable to nonspherical particles. To determine this requires generalizing from a large amount of experimental data and calculations. We summarize

below the similarities and differences between scattering by spherical and nonspherical particles, based on the work cited in this chapter, in the hope that it will provide guidelines to the judicious use of Mie theory.

1. Scattering by single, or collections of oriented, nonspherical particles may, unlike scattering by spheres, be azimuthally dependent.
2. Large nonspherical particles scatter similarly to area-equivalent spheres near the forward direction.
3. Rainbow angles are not evident in matrix elements for nonspherical particles.
4. The scattering diagram (incident unpolarized light) for nonspherical particles tends to be flatter than that for spheres at angles greater then about 90°.
5. Scattering matrix elements off the block diagonal are zero for mirror-symmetric collections of randomly oriented particles, as they are for spheres.
6. S_{21}/S_{11} for nonspherical particles tends to be opposite in sign to that for spherical particles.
7. The inequalities $S_{22} \leqslant S_{11}$ and $S_{33} \neq S_{44}$ hold for nonspherical particles. The first inequality implies that the cross polarization does not necessarily vanish.
8. There is some evidence that S_{34}/S_{11} for spherical and nonspherical particles are in better agreement than other normalized matrix elements.

If there is one succinct conclusion to be made it is that nonspherical particles and area-equivalent spheres scatter similarly near the forward direction, but differences between the two tend to increase with increasing scattering angle.

NOTES AND COMMENTS

A good discussion of measuring angular scattering by particles is given by Stacey (1956). Techniques of particle production, as well as a wealth of information about the physical properties of particles, are discussed by Green and Lane (1964) in their superb book. Another good source of information about particles is *The Particle Atlas* (McCrone and Delly, 1973abcd; McCrone et al., 1979; McCrone et al., 1980).

For various reasons the microwave analog technique has seen only intermittent use in the United States since its inception over 20 years ago. But recently there has been an upsurge of activity—a hopeful sign. Some of the most recent measurements have been reported by Schuerman et al. (1981).

Additional measurements of the S_{34} matrix element for biological particles (red blood cells) have been reported by Kilkson et al. (1979).